THERMAL ENERGY STORAGE USING PHASE CHANGE MATERIALS IN CORRUGATED COPPER PANELS

A Thesis

by

CLIFFORD OKHUMEODE AIGBOTSUA

Submitted to the Office of Graduate Studies of
Texas A&M University
in partial fulfillment of the requirements for the degree of

MASTER OF SCIENCE

May 2011

Major Subject: Mechanical Engineering

Thermal Energy Storage Using Phase Change Materials in Corrugated Copper Panels

THERMAL ENERGY STORAGE USING PHASE CHANGE MATERIALS IN CORRUGATED COPPER PANELS

A Thesis

by

CLIFFORD OKHUMEODE AIGBOTSUA

Submitted to the Office of Graduate Studies of
Texas A&M University
in partial fulfillment of the requirements for the degree of

MASTER OF SCIENCE

Approved by:

Chair of Committee,	Jorge Luis Alvarado
Committee Members,	David E. Claridge
	Jeff S. Haberl
Head of Department,	Dennis O' Neal

May 2011

Major Subject: Mechanical Engineering

ABSTRACT

Thermal Energy Storage Using Phase Change Materials in Corrugated Copper Panels.

(May 2011)

Clifford Okhumeode Aigbotsua, B.Sc, University of Lagos, Nigeria

Chair of Advisory Committee: Dr. Jorge Luis Alvarado

Thermal energy storage systems, precisely latent thermal energy storage (LTES), are systems capable of recovering and storing thermal energy from waste processes, including hot exhaust gases out of combustion engines, or even renewable sources of energy like solar energy. LTES rely on phase change materials (PCMs) to store a significant amount of thermal energy in a relatively small volume. With limited volume and at almost constant temperature, they are capable of storing a large amount of thermal energy, mainly latent energy. Studies of LTES systems have focused primarily on system and process optimization including transient behavior as well as field performance. A major drawback in the development of the use of PCM in LTES has been the low thermal conductivity characteristic of most PCMs. Thus, there is a need to enhance heat transfer using reliable techniques, with the goal of reducing the charging and discharging times of PCM in LTES systems.

Some approaches that have been studied in the past include use of finned tubes, insertion of metal matrix into PCM, and microencapsulation of PCM. The performance of TES configurations in forced convection have been characterized using Reynolds

numbers (Re), and Stefan numbers (Ste) of the heat transfer fluid (HTF) for different enhancement techniques. The goal of this study is to experimentally investigate the effectiveness of corrugated PCM panels with high surface-to-volume ratio in forced convection as a function of HTF mass flow rate, charging temperature, and flow direction through a corrugated TES unit. The PCM (octadecane) has been segmented using sealed corrugated panels containing several channels immersed in the HTF stream. With this approach, the author expects that the charging and discharging times will be substantially reduced due to the high surface-to-volume ratio of the PCM panel for heat transfer. Of the three conditions examined, the HTF direction influenced the charging and discharging times the most with significant reductions in these times observed when the HTF flow direction through the TES was upwards. Buoyancy effects, observed at high Stefan numbers, were important during the charging (melting) process and greatly influenced the temperature profiles along each channel. Results indicate that the devised TES is more effective than some other TES systems in the literature.

ACKNOWLEDGEMENTS

I would like to thank my committee chair, Dr. Jorge Alvarado, for his guidance throughout the course of this research, and my committee members, Dr. D. Claridge, and Dr. J. Haberl, for their extended support in this research. Big thanks also go to Dr. W. Heffington for his moral support throughout my graduate program.

Thanks also go to my friends and colleagues and the department faculty and staff for making my time at Texas A&M University a great experience. I would like to thank a very good friend, Bhanesh Akula, for his encouragement and support throughout the project. Special thanks to Mr. William Seward for his help in the hardware machining.

Finally, I want to say a big thank you to my parents, Mr. and Mrs. Anthony Aigbotsua, and siblings, Nelson Aigbotsua, and Anthonia Aigbotsua, for their encouragement, moral support, and love throughout the graduate program.

TABLE OF CONTENTS

LIST OF FIGURES

FIGURE Page

FIGURE Page

LIST OF TABLES

CHAPTER I

INTRODUCTION

Scientists all over the world are in search of new and renewable energy sources to reduce the CO_2 emissions from the combustion of fossil fuels. The United States and other developed countries are trying to reduce their dependence on oil imports from other countries by considering renewable sources of energy like solar energy which has an enormous potential for the heating and cooling of buildings, producing hot water for domestic and industrial purposes, cooking, warming greenhouses for agricultural crops, etc. However, solar energy is intermittent, unpredictable, and available only during the day. Hence, its application requires efficient thermal energy storage so that the surplus heat collected during daylight hours may be stored for later use at night. Similar situations are dominant in industrial heat recovery systems where the waste heat availability and utilization periods do not coincide, leading to the need for energy storage. These among other factors like escalating energy costs have warranted research in the area of thermal energy storage.

Thermal Energy Storage (TES) is simply the storage of thermal energy in a medium that allows dense energy storage for later use, and it is classified into two categories: sensible heat storage which involves the temperature variation of a material, and latent heat storage which is a storage system that utilizes a materials ability to change phase at almost constant temperature.

This thesis follows the style of Applied Thermal Engineering.

This technology is widely applied in space solar power generation (Kerslake and Ibrahim [1]), HVAC applications (e.g. absorption chillers), district cooling in military installations, and electricity demand side management (as in building thermal insulations).

1.1 Thermal energy storage

Thermal energy can be stored as internal energy in a material either as sensible heat, latent heat, thermo-chemical heat, or a combination of these. Described ahead are the major two classifications of thermal energy storage.

1.1.1 Sensible thermal energy storage (STES)

It is known that all substances can store a certain amount of heat. This property exhibited by all matter is called thermal capacity. When a solid is heated, it experiences an increase in temperature until the melting point is attained. Below the melting point, there exists no phase change of the material. The heat responsible for this temperature increase is called the sensible heat and it is proportional to the difference between the attained temperature and the initial temperature, the mass of the solid, and its heat capacity all related by the equation:

$$Q = \int_{T_i}^{T_f} m.c_v dT = m.c_v\left(T_f - T_i\right) \qquad (1)$$

where,

Q is the heat stored (Joules)

m is mass of media (kg)

c_p is the specific heat at constant pressure (kJ/kg.K)

T_i is the initial temperature of medium (K) and

T_f is the final temperature (K)

Typically, a sensible thermal energy storage system consists of an insulated tank which holds the storage medium and consequently the thermal energy, the storage medium (e.g. water or for absorbing thermal energy), and the input and output hardware such as piping to allow for the transfer of energy in and out of the storage tank.

1.1.2 Latent heat storage (LHS)

The heat required to transform a substance from one phase to another at almost constant temperature is called the latent heat. The latent heat is much higher than the sensible heat change for a given medium, and it is also attractive for most applications because of its high energy storage density requiring only small temperature variations (Lane [2]; Abhat [3]). Latent heat storage has been researched and pioneered by Dr. Telkes in the 1940s (Lane [2]) and others. It did not receive much attention until the energy crisis of the late 1970s and 1980s when it was researched for use in different applications especially for solar heating. The first application of PCM described in literature was their use for the heating and cooling of buildings by Telkes [4].

The storage capacity of a LHS system incorporating a PCM medium is given by

$$Q = m.\varphi.\lambda + \int_i^m m.c_{sp}dT + \int_m^f c_{lp}dT$$

$$Q = m.\left(\varphi.\lambda + c_{sp}\left(T_m - T_i\right) + c_{lp}\left(T_f - T_m\right)\right) \qquad (2)$$

where,

m is the mass of heat storage medium (kg)

c_p is the specific heat capacity (kJ/kg-K)

c_{lp} is the average specific heat between T_m and T_f (kJ/kg-K)

c_{sp} is the average specific heat between T_i and T_m (kJ/kg-K)

T_f is the final attained temperature (^oK)

T_i is the initial temperature of the medium (^oK)

T_m is the melting temperature (^oK)

λ is the heat of fusion (kJ/kg)

φ is the melted fraction

Amongst the thermal storage techniques mentioned above, the LHS is most attractive due to its advantages of high energy storage capacity per unit volume, small thermal gradients during charging and discharging, the possibility of simultaneous charging and discharging with the appropriate selection of heat exchanger, and also charging and discharging of energy at almost constant temperature. LHS systems consist of a heat exchanger surface for transferring heat from the heat source to the heat storage substance (the PCM) and vice versa. The heat exchanger surface itself plays an important role in the design of LHS systems, as it strongly influences the temperature gradients for charging and discharging. Proper design of such systems involves the suitable selection of materials for the heat transfer surfaces, system geometry, and PCM for the application.

PCMs either undergo solid-solid, liquid-gas, and solid-liquid phase transformations. Relatively few solid-solid PCMs have been identified that have heats of fusion and transition temperatures suitable for thermal storage applications. Solid-gas and liquid-gas transition have a higher latent heat of vaporization which requires large volume changes during phase transition limiting their potential use in thermal storage systems. In addition, large changes in volume make the system complex and impractical. Therefore, the only two thermal energy storage approaches of practical interest are those that rely on solid-liquid and solid-solid transformations (Wang et al. [5]).

In solid–solid transitions, heat is stored when the material is transformed from one crystalline state to another. This transition generally has smaller latent heat and volume changes than solid–liquid transition (Sharma and Sagara [6]). Solid–solid PCMs offer the advantages of less rigorous container requirements and better design flexibility. Liquid-gas PCMs usually have high melting temperatures; however, due to the large volume change during transformation, they are not usually considered for practical applications. Solid–liquid transformations have relatively smaller latent heat than liquid-gas but these transformations involve only a small change in volume less than 10 % [6]. Solid-liquid transition has proved to be economically attractive for use in thermal energy storage systems [6].

A heat transfer medium is required to transfer energy from the thermal source to the PCM and from PCM to the load. Therefore, designing a suitable heat exchanger is an important part for improving heat transfer in latent heat storage systems. PCMs also

have positive volumetric expansion on melting, so, the containers must be designed to accommodate this expansion. Any latent heat storage system must possess at least the following three properties: a suitable PCM with its melting point in the desired temperature range for a given application, a suitable heat exchanger surface, and a suitable container compatible with the PCM. A survey of previous literature dealing with LHTES shows that the two common geometries employed as PCM containers include rectangular and cylindrical configurations. The most analyzed configuration is the shell and tube system, accounting for more than 70% of the systems used today, probably due to the fact that most systems use cylindrical pipes with minimal heat losses when compared to other systems (Agyenim et al. [7]). Typically, PCM is placed in the hollow space between two concentric tubes as shown in Fig. 1. During a heat storage cycle, a hot fluid called the heat transfer fluid (HTF) is pumped through the inner tube. This causes some melting in the PCM via the storage of sensible and latent heats. During the heat recovery cycle, the circulation of a low temperature fluid through the same inner tube absorbs the stored energy thereby causing the solidification of the PCM.

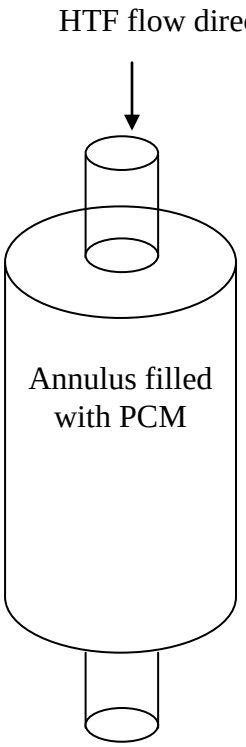

Fig. 1 A shell and tube LHTES unit

1.2 Latent heat storage materials

Phase Change Materials (PCM) are substances with high latent heat of fusion which are capable of storing and releasing large amounts of energy during melting and solidification, respectively, with most of the energy exchange taking place during the latent stage. During the solid-liquid phase change transition, the PCM absorbs heat until it completely melts. The temperature remains relatively constant until the melting process is finished. The heat stored during the phase change process (melting process) of the material is called latent heat of fusion. To date most of the studies conducted on storage materials have concentrated on sensible and latent heat storage systems. Studies

conducted to compare PCM and sensible heat storage materials have shown that a relatively significant reduction in storage volume can be achieved using the former. Morrison and Abdel-Khalik [8] showed that to store the same amount of energy from a solar unit collector area, a sensible heat storage material requires more than seven times the storage mass of Paraffin 116 Wax, five times the storage mass of medicinal paraffin, and more than eight times the storage mass of $Na_2SO_4.10H_2O$. In general, latent heat storage results in energy storage densities typically 5 to 10 times higher than that of sensible heat storage for a PCM. Latent heat storage materials can be used in a wide temperature range of applications.

Thermal energy storage systems should consider the thermo-physical, kinetic and chemical properties (Hale et al. [9], Garg et al. [10], Buddhi and Sawhney [11]) of PCM during the design phase. The most important thermo-physical properties are:

- Melting point
- High latent heat of fusion per unit volume
- High specific heat
- High thermal conductivity in the solid and liquid phases
- Small volume changes on phase transformation and small vapor pressure at operating temperatures
- Completely reversible melting and crystallization of PCM

The kinetic properties of interest are:

- Heterogeneous nucleation to avoid the super cooling effect of the liquid phase
- High rate of crystal growth, so that the system can meet demands of heat recovery

from the storage system

In addition, the PCM must also be

- Chemically stable

- Possess chemical stability after a large number of freezing/ melting cycles with no chemical decomposition

- Non-corrosive to the construction materials

- Non-toxic, non-flammable, and non-explosive for safety

Moreover, low cost and large-scale availability of the PCMs is also very important

1.3 Classification of PCMs

Classification of PCMs is given in Fig. 2. Generally, PCMs are classified based on their melting point range and also their latent heat of fusion. However, except for the melting point in the operating range, the majority of phase change materials do not satisfy the criteria required for an adequate storage media. As no single material can have all the required properties for an ideal thermal-storage medium, one has to use the available materials and try to make up for the poor property by having an adequate system design. For example, metallic fins can be used to increase the thermal conductivity of PCMs; super cooling may be suppressed by introducing a nucleating agent in the storage material, and incongruent melting can be inhibited by use of suitable material thickness. In general, inorganic compounds have almost double the volumetric latent heat storage capacity (250–400 kg/dm^3) of the organic compounds (128–

200kg/dm^3). Inorganic compounds include salt hydrates, salts, metals and alloys, whereas organic compounds are comprised of paraffin, non-paraffin and polyalcohols.

A classification of PCMs used for LHS systems is shown in Fig. 2 below.

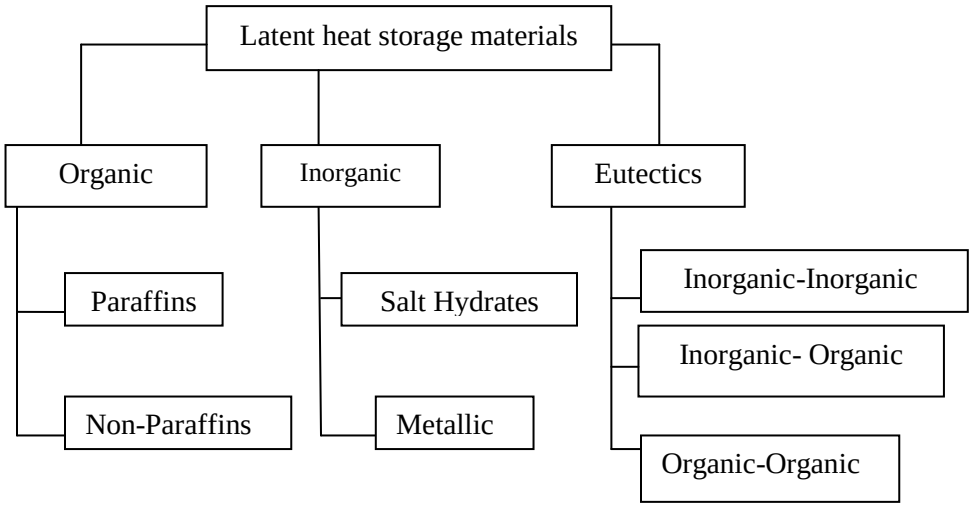

Fig. 2 Classification of latent heat storage materials

A detailed description of suitable PCMs can be found in the literature review section.

CHAPTER II

LITERATURE REVIEW

In this order, this chapter details the different types of PCMs applied in TES, some TES applications, the heat transfer mechanisms in TES, and the different enhancements for improved performance that have been studied in the past.

2.1 PCMs of major interest

2.1.1 Paraffin

The normal paraffins of type C_nH_{2n+2} are a family of saturated hydrocarbons with very similar properties. Paraffins between C_5 and C_{15} are liquids. Paraffin wax is the most-used commercial organic heat storage PCM (Lane [2], Hale et al. [9]). It consists of mainly straight chain hydrocarbons that melt around the range from 23 to 67 ^oC (Abhat, [3]). Properties of some paraffins are given in Table 1. In general, the longer the average length of the hydrocarbon chain, the higher the melting temperature and heat of fusion (Hiran et al. [12]). Paraffins have been found to exhibit many desirable characteristics as PCMs for storage applications, such as high latent heat of fusion, negligible supercooling, low vapor pressure in the melt, chemically inert and stable self-nucleating capabilities, no phase segregation, and commercially available at relatively low cost (Lane [2], Abhat [3], Hasnain, [13]). However, in spite of their many desirable properties, they have some undesirable properties such as low thermal conductivities and large volume change during phase transition. Metallic fillers, metal matrix structures,

finned tube and aluminum shavings have been used to improve their thermal conductivity. To overcome the volume change problem during melting and freezing,

Table 1. Melting point and latent heat of fusion of paraffins

Name	No. of "C" atoms	Melting Point (^oC)	Density (kg/m^3)	Thermal Conductivity (W/m-K)	Latent Heat (kJ/kg)
n - Dodecane	12	-12	750	0.21^S	n.a.
n -Tridecane	13	-6	756		n.a.
n - Tetradecane	14	4.5-5.6	771		231
n - Pentadecane	15	10	768	0.17	207
n - Hexadecane	16	18.2	774	0.21^S	238
n - Heptadecane	17	22	778		215
n - Octadecane	18	28.2	814^L, 775^L	0.35^S, 0.149^L	245
n - Nonadecane	19	31.9	912^S, 769^L	0.21	222
n - Eicosane	20	37			247
n - Heneicosane	21	41			215
n - Docosane	22	44			249
n - Tricosane	23	47			234
n - Tetracosane	24	51			255
n - Pentacosane	25	54			238
Paraffin wax	n.a.	32	785^S, 749^L	0.514^S, 0.224^L	251
n - Hexacosane	26	56	770	0.21^S	257
n - Heptacosane	27	59	773		236
n - Octacosane	28	61	910^S, 765^L		255
n - Nonacosane	29	64			240
n - Triacontane	30	65			252
n - Hentriacontane	31	n.a.	930^S, 830^L		n.a.
n - Dotricontane	32	70			n.a.
n - Triticontane	33	71			189

S: solid; L: liquid; n.a.: not available
Source: Sharma and Sagara [6]

different geometry containers have been used. Some of the paraffins investigated for heat storage applications include commercial waxes, n-eicosane, and n-octadecane (Hasnain [13]).

2.1.2 Non-paraffins

This category includes a wide variety of organic materials such as fatty acids, alcohols, esters, and glycols. Fatty acids have melting temperatures suitable for heating applications and have heat of fusion values comparable to those of paraffins and salt hydrates (Markley [14], Weast and Astle [15]). They are flammable and should not be exposed to excessively high temperatures, flames or oxidizing agents. One promising use, proposed by Kauranen et al. [16], is a system that combines fatty acids to obtain melting temperatures ranging from 20 – 30^{o}C with an accuracy of ±0.5^{o}C. This would be beneficial during design of thermal systems in that it would allow a designer to select the optimum operating temperature to obtain the maximum performance of a heat storage system. Their major drawback is cost which is about three times more than paraffins (Hasnain [13]). Table 2 is a list of some common fatty acids and their thermo-physical properties.

Table 2. Melting point and latent heat of fusion of fatty acids

Name	Melting Point (^{o}C)	Density (kg/m^{3})	Thermal Conductivity (W/m-K)	Latent Heat (kJ/kg)
Proplylpalamiate	10	n.a.	n.a.	186
Isopropyl palmiate	11	n.a.	n.a.	100
Oleic acid	13.5-16.3	863^{60C}	n.a.	n.a.
Vinyl stearate	27-29	n.a.	n.a.	122

Table 2. Continued

Name	Melting Point (^oC)	Density (kg/m^3)	Thermal Conductivity (W/m-K)	Latent Heat (kJ/kg)
Dimethyl sabacate	21	n.a.	n.a.	120-135
Methyl palmitate	29	n.a.	n.a.	205
Capric acid	32	878^{45C}	$0.153^{38.5C}$	152.7
	31.5	886^{40C}, 1004^{24C}	0.15255.5C, 0.149^{40C}	153
Erucic acid	33	853^{70C}	n.a.	n.a.
Methyl-12-hydroxy-stearate	42-43	n.a.	n.a.	120-126
Lauric acid	42-44	862^{60C}, 1007^{24C}	n.a.	178
Elaidic acid	47	851^{55C}	n.a.	218
Pelargonic acid	48	n.a.	n.a.	n.a.
Myristic acid	49-51	861^{55C}	n.a.	205
	54	844^{80C}		187
Palmitic acid	64	850^{65C}	$0.162^{68.4C}$	185.4
	61	847^{80C}	$0.159^{80.1C}$	203.4
Stearic acid	69	848^{70C}	0.172^{70C}	202.5
	60-61	965^{24C}		186.5
Valporic acid	120	n.a.	n.a.	n.a.

S: solid; L: liquid; n.a.: not available
Source: Sharma and Sagara [6]

2.1.3 Salt hydrates

Salt hydrates are the oldest and most studied heat storage PCMs (Lane [2]). They consist of salt and water, which combine in a crystalline matrix when the material undergoes solidification. They are also the most important group of PCMs, and have been extensively studied for their use in LHS (Sharma and Sagara [6]). Their advantages include low cost, availability, sharp melting point and high and high thermal

conductivity when compared with other heat storage PCMs, facilitating heat transfer in and out of a storage system. They possess a low volume change during phase transformation and also have a high heat of fusion, thereby reducing the system size and make it easy to design a container that could accommodate volume change. Two of the inexpensive and most available salt hydrates are $CaCl.6H_2O$ and $Na_2SO_4.10H_2O$ (Lane [2]). One of their major disadvantages is degradation after a substantial number of cycles. Abhat [3] reports a decrease in the heat of fusion by over 73% in $Na_2SO_4.10H_2O$ after 1000 melting/freezing cycles. Lane [2] suggests this problem could be reduced by using gelled or thickened mixtures, although Abhat [3] predicts this process negatively influences the heat storage characteristic of the mixture. Another disadvantage is the possibility to cause corrosion in metal containers, which are commonly used in thermal storage systems [3]. Thus the compatibility between a PCM and its container must be investigated during the design phase of the system.

2.1.4 Eutectics

They are mixtures of two or more salts with the possible lowest melting temperature, each of which melt and freezes congruently, forming a mixture of crystals during crystallization (Lane [17]). This class of PCMs nearly always melts and freezes forming a homogenous mixture of crystals resulting in a limited phase separation of the constituent components. An example of an eutectic used as a potential candidate for space heating and process heat applications is the eutectic combination of

pentacrythricol ($C_5H_{12}O_4$), pentaglycerine (CH_3-C-(CH_2-OH_3)) and neopentyl glycol ((CH_3)$_2$-C-(CH_2OH)$_2$) (Lane [17]).

2.2 Some TES applications and uses

2.2.1 Construction materials

Electrical energy consumption varies significantly during the day and night according to the demand by industrial, commercial and residential activities, especially in extremely hot and cold climate countries where the major part of the variation is due to domestic space heating and air-conditioning. Because of the low thermal mass of light weight building materials, they tend to have high temperature fluctuations, which result in high heating and cooling demands. Such variation leads to a differential pricing system for peak and off peak periods of energy use. Significant economic benefit can be achieved if some of the peak load can be shifted to the off peak load period, with the help of thermal energy storage. PCMs have been considered for thermal storage in buildings since 1980 and are now being inserted in building materials like gypsum board, plaster, concrete or other wall covering material (Neeper [18]). By absorbing heat during peak time (e.g. during sunshine) and delaying its release at night, building energy demand can be somewhat controlled which should result in huge energy cost savings for some large building applications. Neeper [18, 19] examined the thermal dynamics of gypsum wallboards impregnated by fatty acids and paraffin waxes as PCMs that are subjected to the diurnal variation of room temperature. They found that the thermal storage provided by PCM–wallboard would be sufficient to enable the capture of large

solar heating fractions. However, the development of reliable and practical thermal energy storage systems still face some major hurdles, such as uncertainties concerning the long term thermal behavior and the small number of PCMs suitable for room temperature applications.

2.2.2 Electronic cooling

Electronic components like handsets, portables and power electronics are known to fail when their application or environmental conditions exceed the application limit. A survey from the US Air Force [20] shows that the percentage of temperature related failures in electronics exceeds 55%. This high percentage is evidence that the current cooling methods are inadequate to fulfill the device cooling need. A lot of research has been done (Esam and Amon [21]) and is still ongoing on how this problem could be curtailed. Thermal control units (TCU) have been developed to improve thermal management of electronic devices where their operating time is limited to few hours. The TCU is composed of a PCM and a thermal conductivity enhancer (TCE). The TCU's primary function is to absorb the excessive heat that is generated in the heat source component during operation by allowing the PCM to melt, and then release it during OFF time while keeping the electronic outer surface temperature relatively low and comfortable to the user's skin. Once the component temperature reaches the PCM melting temperature, the PCM absorbs heat until it completely melts. During this period, the component temperature is almost constant and a temperature rise is delayed,

allowing additional operating time before reaching the component's maximum temperature.

2.2.3 Space exploration

Electrical power for NASA's space station Freedom is generated by photovoltaic solar arrays and augmented by solar dynamic power modules (SDPM's). The SDPM employs a concentrator to collect and focus solar energy on the walls of a cylindrical cavity heat receiver where it is converted to thermal energy. A fraction of the thermal energy is converted and transferred to a circulating working gas to operate a heat engine for electrical power generation. The other fraction of energy is used to melt a eutectic composition LiF-CaF_2 phase change material contained in multiple canisters located concentrically around working fluid tubes running the length of the heat receiver cavity. The PCM stores and releases thermal energy by undergoing phase change at its critical temperature of 1040K. This permits continuous operation of the heat engine during substantial eclipse periods of Freedom's low earth orbit.

2.2.4 Agriculture

Drying of agricultural products in some developed and developing countries constitutes a huge portion of energy consumption considering both commercial and non-commercial energy sources. Utilization of solar energy for thermal applications, like cooking, heating and drying, is well recognized in tropical and semitropical regions. Agricultural products (e.g. cereals, pulses, foods and vegetables) are usually preserved at

almost constant temperature and continuously for few days making it an application amenable to thermal energy storage. In such scenarios, a thermal storage system incorporating a solar heat source could be used. However, solar energy is intermittent by nature; its availability is seasonal and dependent on the meteorological conditions of a particular location. For agriculture purposes, unreliability is the biggest hindering factor for extensive solar energy utilization and could be reduced by storing a portion when it is in excess of the thermal load and using the stored energy later when needed. Energy storage is therefore essential to any system that depends largely on solar energy. It adjusts temporal mismatches between the load and the intermittent or variable energy source, thereby improving the system operability and utility.

2.3 TES thermal enhancement techniques considering heat transfer mechanisms of PCMs

In spite of their desirable properties, the major problem common to all PCMs is their low thermal conductivity which presents a huge challenge in the design of heat storage systems, and in turn limits their use. The effect of low conductivity in PCMs is important in the discharging (solidification) process (Jegadheswaran and Pohekar [22]). This is particularly relevant when the PCM is in the liquid state since the thermal conductivity is lower than in the solid state. As a result, the thermal resistance within the PCM during solidification is more than that during the melting process causing the solidification process to be mainly conduction-limited. Thus, improving the thermal performance of these materials through TES geometrical reconfiguration should improve

heat transfer and reduce the charge and discharge times making them useful in applications where charge and discharge times are of the essence. Various heat transfer enhancement techniques for LHS systems have been suggested and are enumerated below:

1. Thermal conductivity enhancement
2. Extended surfaces
3. Micro-encapsulation of PCM
4. Use of multiple PCMs

The governing (and dominating) heat transfer mechanisms in LHS systems differ with the type of phase change processes that take place (melting and solidification). Moreover, these mechanisms greatly depend upon the system's configuration (cylindrical or rectangular) and orientation (horizontal, vertical or inclined). Sequentially, the proceeding discussion describes melting (and the significance of natural convection), solidification (and conduction), and some recent studies relevant to the theme of this thesis that have to do with cylindrical LHS systems (2^{nd} and 4^{th} enhancement techniques).

2.3.1 Melting of PCM in TES units

The first mode of heat transfer in the PCM is conduction during the initial phase of melting, and later by natural convection. As heat transfer progresses, the thickness of the melted PCM increases, and the solid region moves away from the heat transfer surface. Since a PCM in its liquid phase has a lower thermal conductivity than the solid

phase, the heat transfer by conduction ceases to be the only heat transfer mechanism of importance. In fact, natural convection becomes a dominant heat transfer mechanism due to the presence of density gradients within the melted PCM.

Lamberg et al. [23] conducted numerical and experimental studies on melting of paraffin in rectangular enclosures with and without consideration of natural convection effects, and the results were compared to experimental results. They used two numerical methods (enthalpy and effective heat capacity) to understand the role of natural convection. Both numerical methods gave almost identical results and it became evident that incorporating natural convection into the numerical scheme ensured a fairly good estimation of the PCM behavior during melting when compared with experimental results. Furthermore, when the numerical scheme ignored natural convection effects, the calculated time for the PCM to attain the heat source temperature doubled. The results indicated considerable error and the numerical model was not satisfactory (matching wise) if natural convection was not taken into account during the PCM melting.

Stritih [24] experimentally monitored the interface position during melting of paraffin in a rectangular storage system and compared the results with analytical results that were conduction-based (ignoring natural convection effects). He observed that the data showed good agreement with experimental results only at the onset of melting when conduction was dominant. During melting, the experimental interface location was much ahead of the one obtained analytically. He also established a correlation between

the dimensionless numbers (Nusselt number as a function of Rayleigh number) which showed that natural convection was indeed necessary during melting and contributed to enhanced heat transfer.

Zhang et al. [25] studied the melting of n-octadecane in an enclosure with one wall heated by three discrete sources (made of constantan wire) at a constant rate while the other walls were insulated. The time-dependent solid-liquid interface shape was viewed using a He-Ne laser and camera during the melting process. At the beginning of melting, three small isolated melting regions were noticed on PCM adjacent to the heated vertical wall. As time passed, they eventually joined together forming a single region. Natural convection developed in this region which led to the upward movement of the melted PCM generating a convection cell which resulted in the sinking of relatively colder liquid (see Fig. 3). This led to high temperatures near the top of the system. They also observed similar behavior of the solid-liquid interface under different Stefan numbers. However, rapid melting and high melted liquid volumes observed at high Stefan numbers was due to natural convection effects becoming more dominant.

Jellouli et al. [26] studied melting of PCM in a rectangular enclosure heated from below. The isotherms obtained numerically revealed a dominant role of heat transfer by conduction during the initial stage of melting since buoyancy forces could not overcome the resistance imposed by viscous forces. In situations where heat is applied near the bottom of a TES system, usually the cold (melted) PCM layers on top of the warm PCM layers one leads to the development of the thermo-convective instabilities. The zone near the hot bottom side is characterized by steep temperature gradients which initiate and

maintain the natural convection flow within the liquid phase and gradually influences the local heat transfer rate and therefore the melting characteristics of the system.

As is the situation in rectangular enclosures, natural convection has also been found as the dominant heat transfer mechanism in cylindrical and spherical enclosures. Jones et al. [27] performed experimental and numerical studies on the melting of PCM in a cylinder heated from the exterior of the vertical side wall. Initially, they observed a

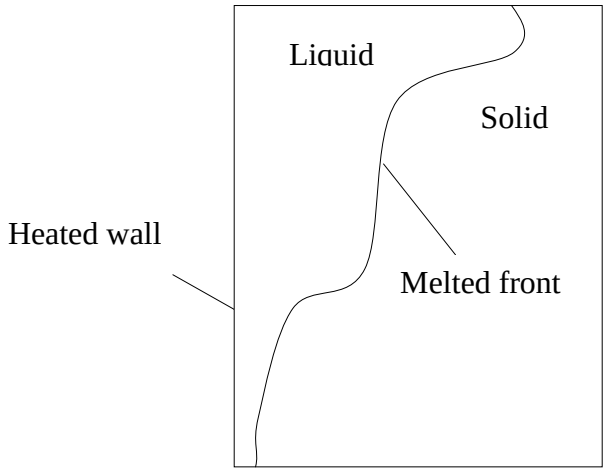

Fig. 3 Natural convection dominated melting process in a rectangular system [25]

nearly uniform molten layer thickness along the vertical direction from photographs taken during the melting process. Since the molten layer thickness was very small, conduction was likely to be the dominant conduction was likely to be the dominant heat transfer mechanism. The melt front shape was similar to the pure conduction regime observed initially in rectangular enclosures [25] during melting. As the melting progressed, the molten layer thickness began to vary along the z-direction (vertical), with the molten layer being thickest at the top of the enclosure as seen in Fig. 4. This

indicated increased buoyancy-driven natural convection effects. As natural convection currents get established, the effects on the solid/liquid interface become more pronounced, eventually varying the melt layer continuously along the height of the cylinder.

Akgun et al. [28] studied the melting process of paraffin stored between the annulus of a tube in shell TES configuration oriented vertically and their observation

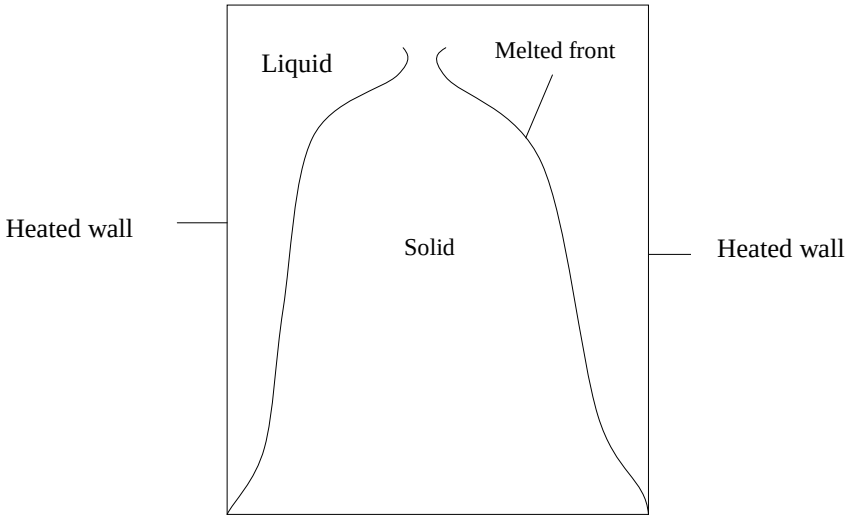

Fig. 4 Natural convection dominated melting process in a cylindrical system [26]

was similar to that of Jones et al.[27]. When the PCM was heated from the inner wall, molten PCM extended radially outward, increasing upwards along the PCM thermal mass, and eventually forming a somewhat conical shape around the heat transfer tube. This was because convection induced buoyancy effects caused the hotter liquids to rise to the top, thus promoting melting in the upper region.

Ng et al. [29] numerically studied the melting of PCM stored in a horizontal cylindrical annulus heated isothermally from the inner wall of the heat transfer tube (Fig. 5) with the outer wall being adiabatic. The natural convection was modeled by the Boussinesq approximation. The results showed recirculation cells which are representations of natural convection flow in the liquid PCM. Heat transfer by conduction played a dominant role in the concentric liquid region that formed around the heated cylinder during initial stages. After some time, the natural convection intensified

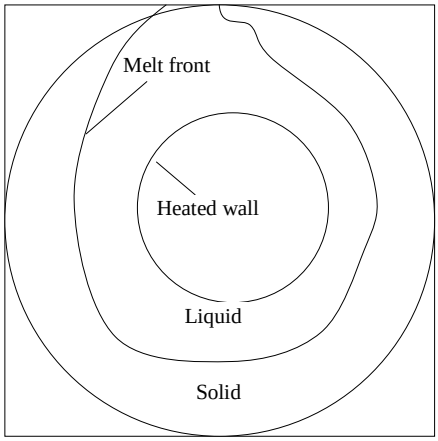

Fig. 5 Natural convection dominated melting process in cylindrical annulus [29]

and it affected the melting front position and consequently resulted in unsymmetrical melting about the axis of the cylinder. The results also showed that melting takes place primarily above the heated cylinder with very little melting occurring below.

Experimental investigations of PCMs around a heated single cylinder (finned and un-finned) or arrays of cylinders were performed by Bathelt et al. [30, 31], Bathelt and Viskanta [32], Yao and Chen [33] and Abdel-Wahed et al. [34]. They all observed

similar melting profiles and also reported the dominance of heat conduction during the early stages of the melted PCM around the un-finned cylinder.

Regin et al. [35] analyzed the melting behavior of paraffin wax encapsulated in a cylindrical capsule surrounded by hot water. The experimental results showed the influence of natural convection on the melting process. Initially, the PCM melt was symmetric about the capsule axis, but as time progressed, natural convection intensified eventually caused an axi-symmetrical melting of the molten PCM about the capsule axis causing more melting in the upper region.

Though a spherical system provides the largest volume per unit surface area, only limited study could be found on their application in LHTS systems [22]. Studies pertaining to spheres can be found in the literature [36, 37, and 38].

2.3.2 Solidification

During the PCM solidification process, it has been observed that conduction plays a dominant role. Natural convection also plays a role at the liquid-solid interface due to temperature difference in the PCM; however, natural convection is less relevant compared to heat conduction (Kroegar and Ostrach [39]). The heat transfer characteristics of PCM during solidification have been explained by many investigators.

Ettouney et al. [40] studied the solidification in a shell and tube heat exchanger and discovered that solidification isotherms were almost parallel to the heat transfer surface. In vertical TES configurations, solidified layers took the shape of the heat

transfer surface whether the direction of HTF was upward or downward. Hence, natural convection effects were found to be negligible.

Stritih [24] compared the conduction based analytical results of solidification in a rectangular storage unit with experimental results and obtained a good agreement between the two. In the case of melting, the natural convection was found to be 10 times lower.

These studies prove that in all configurations of LHTES during solidification, the solidified layers were formed from the heat transfer surfaces and remain parallel to them. Although natural convection exists in the liquid PCM at the earlier stages, it diminishes rapidly as the solidification progresses and the process becomes conduction dominated as the liquid volume becomes smaller with time.

2.4 Heat transfer enhancement techniques in TES systems

Several techniques have been investigated and proposed to improve heat transfer during solidification and in general improve the performance of phase change storage units. They include the use of a multiple PCM TES, finned surfaces within the PCM, PCM enclosed in capsules to reduce heat transfer resistance, and the use of high thermal conductivity porous materials to improve the effective thermal conductivity of the TES. Also, fins have been employed to enhance the solidification rate by improving heat conduction alone. Only related techniques (with regards to this thesis) are discussed.

2.4.1 Multiple PCMs

Attention has been directed to the use of multiple PCM types in TES systems as another attractive performance enhancement technique. In this technique, the TES system is packed with more than one PCM each with different melting points. The heat transfer rate in the TES unit and thus the performance of the system during charging (melting) and discharging (solidification) mainly depends on the difference between the HTF temperature and the melting point of each PCM. If a single PCM is used in the unit, then this temperature difference would obviously decrease in the flow direction of the HTF. This causes a decrease in heat transfer rate and thus poor performance of the unit. If multiple PCMs with different melting points are used, then nearly constant temperature difference can be maintained during the melting process, even though the HTF temperature decreases in the flow direction. This leads to an almost constant heat flux to the PCM. The use of multiple PCMs in the shell and tube TES configuration is illustrated in Fig. 6. The benefit of employing multiple PCMs has been reported by Wang et al. [41]. The authors proposed breaking up the PCMs into smaller cavities to achieve an almost homogeneous phase change process. Though a perfectly homogenous PCM cannot be realized, it was suggested that if PCMs of different phase change temperatures were incorporated in such a way, the phase change rate distribution could become parabolic and favor a nearly homogeneous phase change process. It was also reported that with an early homogeneous phase change process, the phase change time can be reduced considerably. Hence, it can be stated that employing multiple PCMs seems to be a promising way to enhance the performance of the TES system during the

charging and discharging processes. Significant work has investigated the performance enhancement achieved by employing multiple PCMs in different configurations of LHS units. Farid and Kanzawa [42] employed three PCMs of different melting points packed in cylindrical capsules using air as HTF. During the charging and discharging processes about 10% increase in heat transfer rate was obtained with three PCMs as the melting/solidification started in all three PCMs simultaneously, as opposed to a single

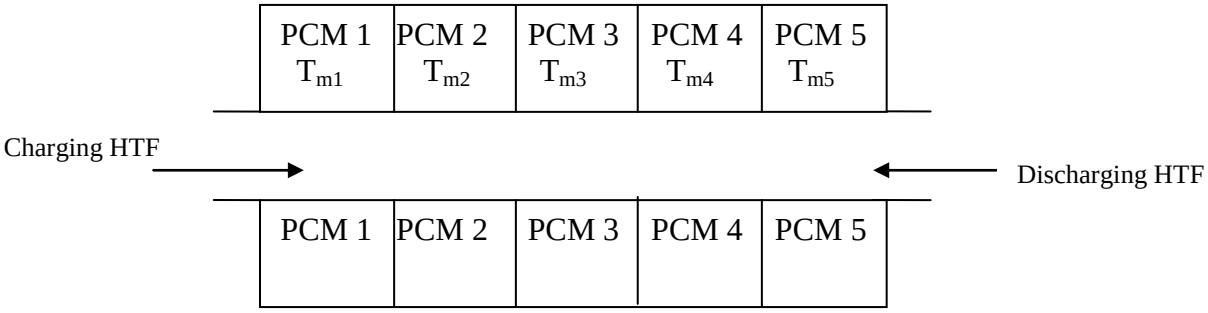

T_m: Melting temperature; $T_{m1}>T_{m2}>T_{m3}>T_{m4}>T_{m5}$

Fig. 6 Multiple PCMs in shell and tube TES

PCM system where the process could have started from the inlet side of the HTF tube and progressed toward the outlet side. Michels and Pitz-Paal [43] revealed the benefit of using multiple PCMs in a shell and tube module. The shell side was loaded with three PCMs and synthetic oil was used as the HTF. It was observed that over a period of time, all three PCMs achieved higher phase change fractions and thus greater storage/discharge capacities compared to the single PCM (of higher melting point) unit. The concept of multiple PCMs has also been extended to the LHS systems for electronic cooling. A study of such system has been undertaken by Wang et al. [44]. It was

reported that if a single PCM were used in the system, then the phase change temperature distribution would have been constant. On the other hand, with multiple PCMs, linear phase change temperature distributions could have been possible. In the systems with constant temperature boundary conditions, a proper arrangement of different PCMs could lead to optimum linear phase change temperature distributions. This resulted in a 25% reduction in phase change time when compared to a single PCM unit. It was also found that enhancement due to multiple PCMs was dependent on the number of PCMs. The authors concluded that the practical and economical number of PCMs might vary from 5 to 10. Seeniraj and Narasimhan [45] also observed a nearly uniform temperature at the HTF outlet for a longer period in a five-PCM shell and tube configuration that for solar TES applications. The multiple PCMs technique has found application in heat receivers of solar dynamic power systems [46, 47].

2.4.2 Use of fins

Fins or extended surfaces have been used to provide additional heat transfer surface in thermal systems. In LHS systems, the role of different configurations of fins in enhancing the performance has been studied extensively by various researchers. The systems using fins, studied until now, are:

- Finned TES system packed with PCM using a HTF
- Finned TES system packed with PCM using a hot/cold boundary wall for heat transfer as seen in electronic cooling applications.

For a TES system that relies on HTF as the heat source, fins are usually located outside the heat transfer tube to improve convection [48]. For a recent review on various kinds of TES proposed by researchers, readers are referred to [49]. Among these, shell and tube/concentric double pipe heat exchangers have been proved to be highly efficient for minimum volume (Lacroix [50]). Few studies have assessed the performance enhancement due to the use of fins in shell and tube/concentric double pipe heat exchangers.

Lacroix [50] developed a three-dimensional numerical model for the melting process in shell and tube LHTS with the PCM on the shell side and the HTF flowing inside. Natural convection was included through an effective thermal conductivity term as a function of Rayleigh number in the conduction equation. The results showed that a large amount of heat was conducted through the fins along the radial direction. For all ranges of mass flow rate and inlet temperature of HTF, a considerable amount of increase in energy stored was observed due to the presence of fins. Increasing the number of fins resulted in an increase in heat transfer rate and thus energy stored at all conditions. The study revealed that heat transfer enhancement when fins were used was dependent on mass flow rate and inlet temperature of the HTF. Maximum enhancement was observed for moderate flow rates and low inlet temperature. On the other hand, for a larger mass flow rate and high inlet temperature of HTF, the enhancement factor was not very significant even with greater number of fins.

A similar configuration was studied by Zhang and Faghri [51]. The numerical study included the effect off in height. It has been shown that the liquid fraction of the

PCM at any time during melting could be increased by increasing the fin height. This is because the melting fronts on both the sides of the fins were greatly affected by the height of the fin although the effect of fins on the melt front was hardly felt between the fins. The investigation also focused on the effect of initial subcooling on the position of melt front and liquid fraction. Generally, many inorganic PCMs show considerable subcooling, which in turn affects system performance [52]. The effect of subcooling on performance when fins were used was almost negligible on both sides of the fins. This clearly shows that the fins were very effective in minimizing unfavorable effects associated with subcooling.

Seeniraj et al. [53] investigated transient behavior of high temperature PCMs stored in a finned tube in shell LHS module that could be used in space based power systems. Since in solar space power systems microgravity conditions prevail, natural convection was assumed to be negligible. The study revealed that if an un-finned tube was used, then some quantity of PCM nearer to the exit of the tube would remain in the solid state. This is because, nearer to the exit, the difference between HTF temperature and the PCM's melting point would be very small. A few annular fins and tubes made of high conductivity materials are capable of causing a relatively higher temperature of the HTF towards the exit in such types of unit. The resulting increase in the difference between the HTF temperature (downstream) and melting temperature of the PCM thus improves the melt fraction at the exit section of the unit. For a fixed size of LHS unit, a significant increase in energy stored was observed due to the presence of fins. However, the increase was substantial only in the initial stages of melting. At any particular time,

the amount of heat transfer was directly proportional to the number of fins; however, adding more fins would have a negative effect on TES heat capacity since more fins mean less PCM. Hence, it was concluded that an optimal number of fins should be identified to be able to transfer and store a significant amount of energy. As reported by Seeniraj et al. [53], heat transfer enhancement decreases as the melting process continues in finned TES systems. This is particularly true in cases of conduction dominated melting. As mentioned earlier, the melting process is dominated by natural convection, making fins particularly attractive during the phase change process.

Most of the previous work in the literature focused on the melting process with particular attention to understanding and proposing ways to enhance the natural convection phenomena. For solidification, as mentioned earlier, conduction is the major mode of heat transfer and thus there is little that can be done to speed up the process. However, few studies have considered the effect of high surface-to-volume ratio TES geometries on both the melting and solidification process. None of the TES geometries studied in the past have used a corrugated geometry. Also to the best of the author's knowledge, none of the systems studied until now have included an inverted flow configuration whereby the HTF flows around the PCM thermal mass. In this study, a TES with such features has been designed using corrugated copper panels (for a high surface-to-volume of PCM), and its thermal response examined. The results show that both the charging and discharging processes were enhanced. For the charging process, the natural convection effects within the PCM were vital, and for the discharging

process, forced convection effects from the HTF (through the large surface area) sped up the process.

CHAPTER III

EXPERIMENTAL DESCRIPTION

3.1 Experimental objective

To design PCM systems requires a good understanding of the fundamental heat transfer processes involved. An accurate understanding of the transient thermal performance of the PCM should be pursued keeping in mind that each TES geometry has a peculiar PCM charging and discharging behavior (i.e. melting and freezing). Among the thermal performance parameters investigated in the literature, melted volume fraction, temperature profile, melting/solidification times, and melting/solidification rate at different Reynolds, Stefan, and Raleigh numbers are important in any TES study. For this study, the effects of varying the Stefan's number (using HTF temperature), Reynolds number (using mass flow rate), and TES orientation on the transient temperature profile of octadecane in a novel type of TES have been investigated. Temperature gradients in the axial and radial directions have been examined to identify the effect of experimental conditions on them. In addition, a dimensionless temperature parameter (θ) was used in estimating a characteristic response time parameter (b) that can be used to compare the devised TES performance to other existing TES systems. The TES system performance has been compared under similar conditions to that of a horizontal multi-tube system investigated by Agyenim et al. [54].

3.2 Experimental setup

A vertical TES system with considerably larger surface-to-volume ratio was designed to determine the effects of high surface-to-volume ratio on the transient thermal response of the PCM. The devised TES was conceptually designed considering different configurations. An inverted configuration consisting of a HTF shell and TES panels enclosing the PCM makes it unique (as illustrated in Fig. 7) since it should result in enhanced thermal transient response. There are a total of six 1ft long corrugated panels joined axially at the TES shell center and positioned at 60 degrees from each other as shown below. The corrugated panel design, see Fig. 9, was chosen for achieving a higher surface area-to-volume ratio. The corrugated panels were made of copper using a plexi glass die and a pressure application device as seen in Fig. 8. Fig. 9 shows the end sections of a single panel. The corrugation profile was chosen in order to achieve

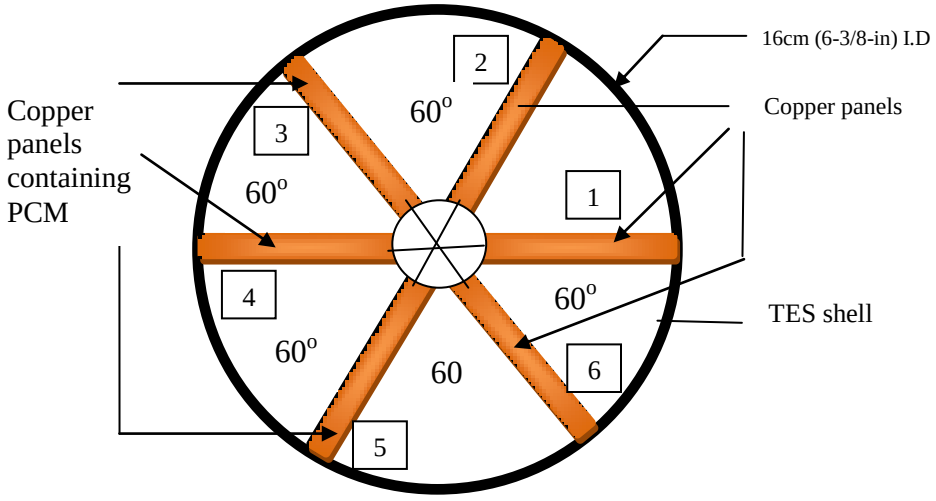

Fig. 7 Top view illustration of TES unit

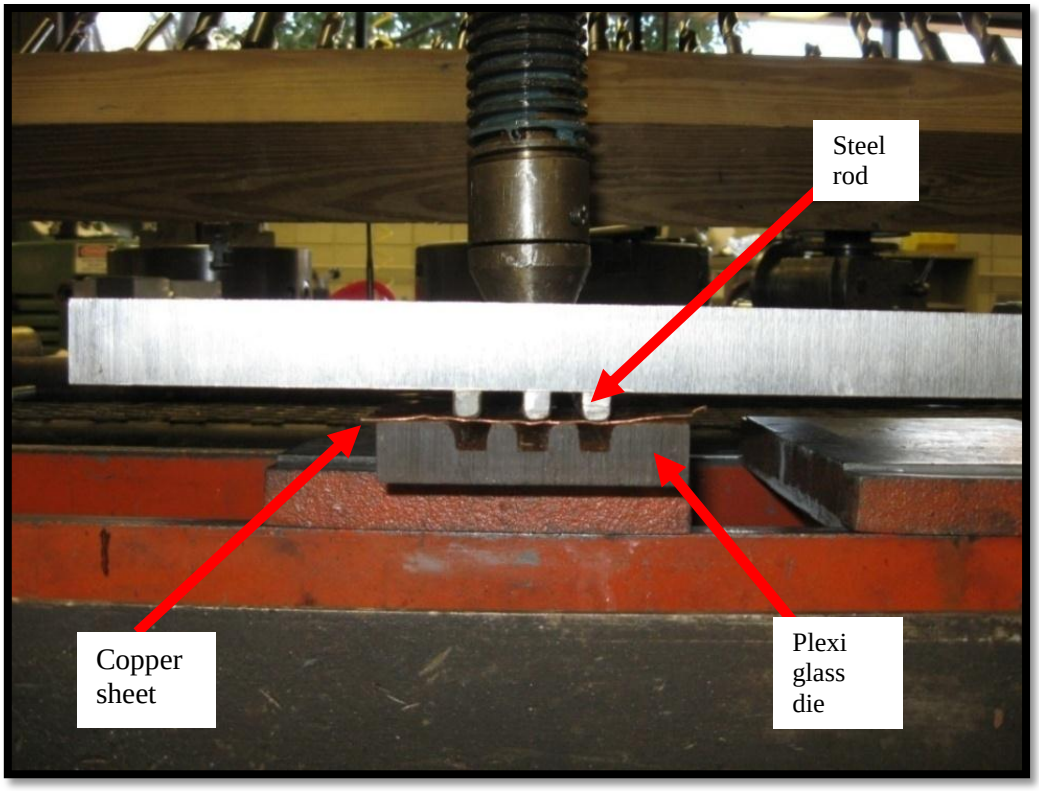

Fig. 8 Panel forming process

two main objectives: (1) high surface-to-volume ratio; (2) enhanced convective heat transport. The unique profile of the TES panel helps promote turbulence within the TES, and resulting in enhanced heat transport. Each panel is made up of six square-cross section channels (A through F) with side 0.8 cm (0.31-in), and a center to center distance of 1.6 cm (0.63-in). 150 cm^3 (150 ml) of melted octadecane was poured into each panel and allowed to solidify before sealing each panel. To avoid large air voids within the PCM panels, a two-step process was followed. First the molten PCM was poured into the each PCM panel until it reached about half the panel length. Then the panel was

dipped into a bucket of ice/water mixture for cooling, and upon cooling, some more PCM was added. The same filling process was done for all the panels.

Shown in Fig. 10 is the TES in the vertical and upright position, including the different thermocouple locations. On the front side of panel 1 are thermocouples A1 through A4, B1 through B3, and C1 through C4. On the back side of panel 1, there are similar arrangements of thermocouples (along channels D, E and F), with D's center about 0.8cm (0.3-in) from the left hand side of pocket C. Channel E's thermocouples are between channels C and B when viewed from the top (as seen in Fig. 9). On the left hand side of the TES is panel 4 with only two thermocouples, G2 and G3, on the front side. There were no thermocouples inserted in panels 2, 3, 5 and 6. Due to the symmetric construction of the TES system, the authors strongly believe the thermal response in each of the six panels will be similar. Moreover, thermocouples G2 and G3 were inserted in panel 4 to validate the assumed symmetrical thermal response of the TES unit. There were a total of 20 thermocouples inserted in panels 1 and 4. Two additional thermocouples were inserted in the upper and lower PVC pipes that conveyed water in and out of the TES unit. The thermocouple wires used were T-type (TT-T-30-SLE) from Omega which were thin enough to avoid the thermocouple fin effect, and also were insulated with PFA (a fluorocarbon polymer). Furthermore, more insulation was applied on all thermocouples using plastic heat shrink tubes to reduce convection effect on the outside of each thermocouple wire. The thermocouple manufacturer, Omega, reports the accuracy of this class of thermocouples to be $\pm 0.5^{o}$C. Identical perforated disks (16 cm diameter, with an open area of 63%) were fixed 15.2 cm (6-in) from both ends of the

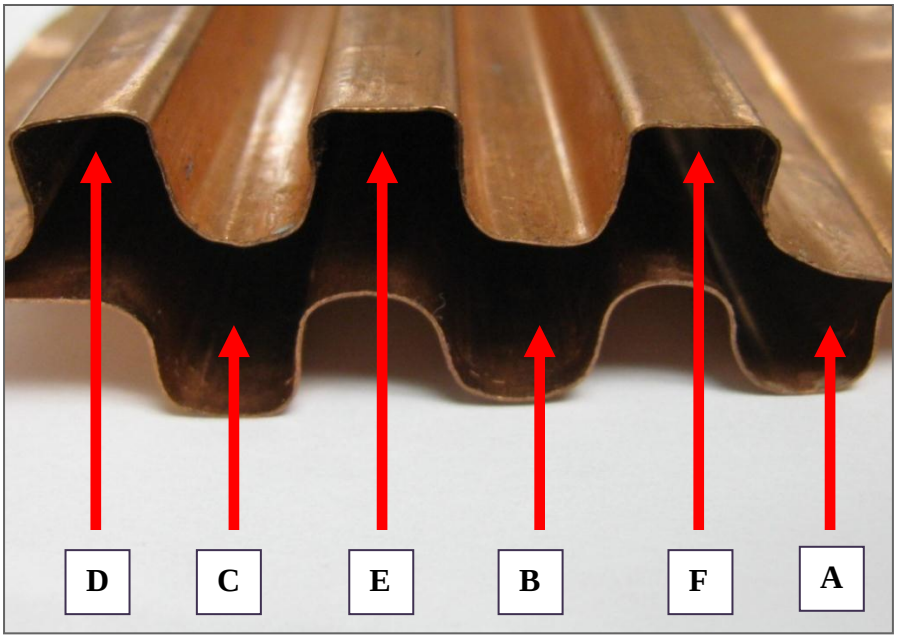

Fig. 9 Top view of a single panel

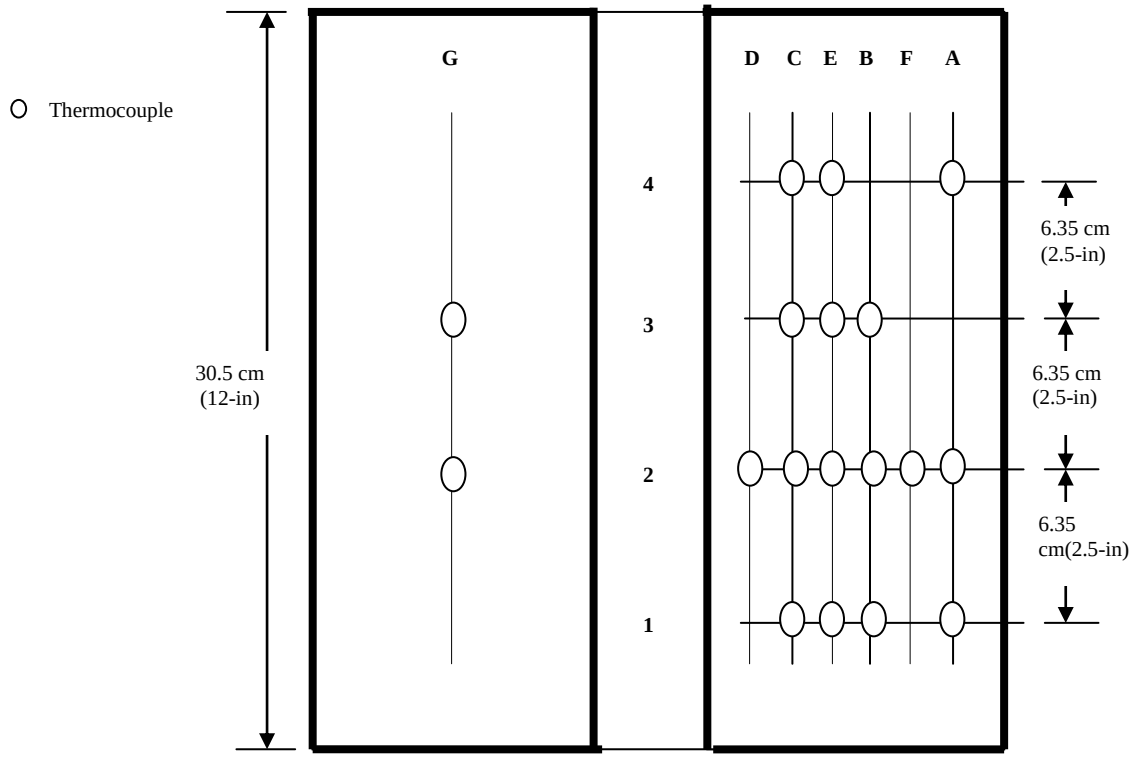

Fig. 10 Side view of panels 4 (Left side) and 1 (Right side) showing thermocouple positions

panels. A picture and illustration of the experimental setup are shown in Fig. 11 and 12, respectively.

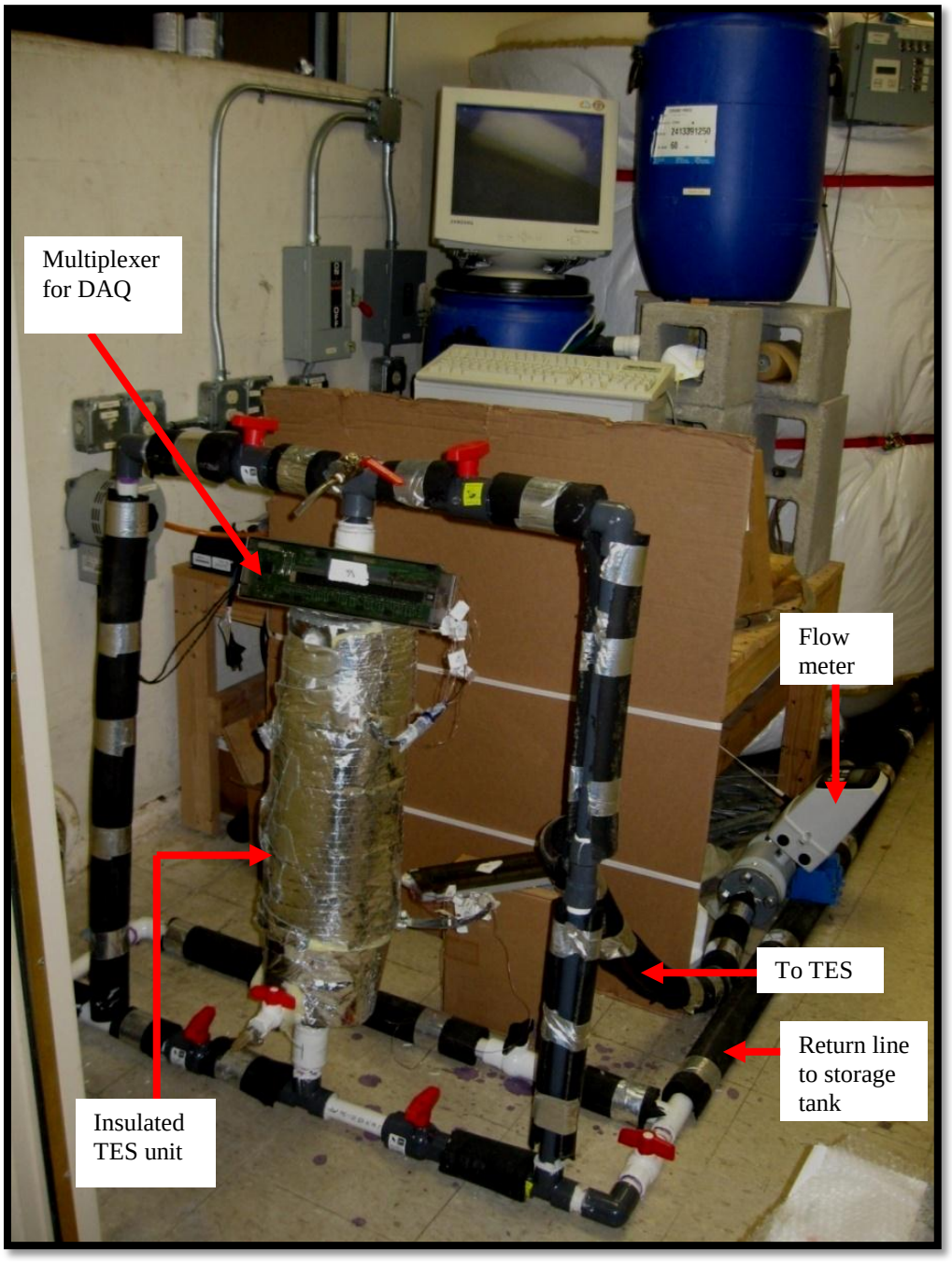

Fig. 11 Picture of experimental setup

The PCM used was 99+% octadecane due to its adequate thermo-physical properties as shown in Table 3. The variation of density, thermal conductivity and specific heat as

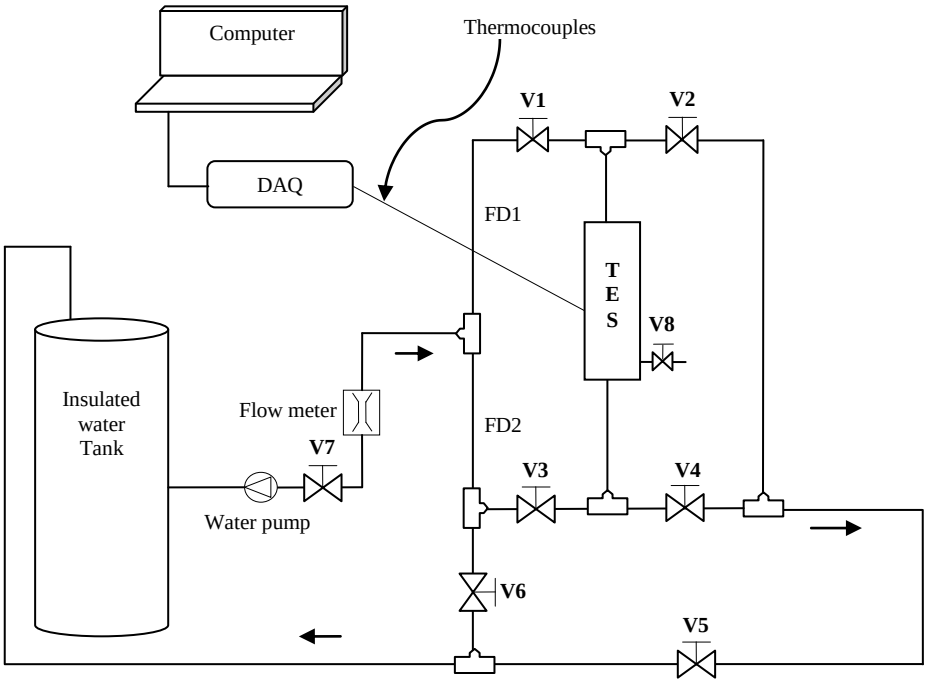

FD 1: TES downward flow direction; FD 2: TES upward flow direction; v: valve
DAQ: data acquisition system
Fig. 12 Schematic diagram of the experimental apparatus

functions of temperature can be found in appendix 1. The corrugated panel assembly was centrally positioned (radially and axially) in an insulated 0.61 m (2ft) long transparent acrylic pipe. Water was used as the HTF and circulated from a storage tank through a 1-in poly vinyl chloride (PVC) pipe network. A Gould pump (model G&L Series) was used to force water through the TES unit. Between the TES and the water storage tank, a flow meter (Siemens FM magflo 5000) was used for flow measurement.

To achieve accurate flow measurement, the flow sensor was installed in a section of straight hose that met the minimum 5-ID upstream and minimum 3-ID downstream as per the manufacturer's requirement. All thermocouple data were recorded using an Agilent 34978-A data acquisition unit, and analyzed using Benchlink data logger software and Microsoft Excel. To maintain axis-symmetric melting in the radial direction in the TES, the experimental setup was oriented in the vertical direction.

Table 3. Thermo-physical properties of 99+% octadecane

Melting/solidification temperature (^{o}C) *	28
Latent heat capacity ($kJkg^{-1}$)*	245
Thermal conductivity ($Wm^{-1}K^{-1}$) solid/liquid***	0.42/0.15
Specific heat ($kJkg^{-1}K^{-1}$) solid/liquid***	1.8/2.2
Density (kgm^{-3}) solid/liquid**	814/775

* Sigma Aldrich website
**Sharma and Sagara [6]
***Shiina and Inagaki [55]

The water tank was well insulated to ensure minimal heat transfer between the tank and the surrounding. Also the tank had about 870 liters (230 gallons) of water during each experiment, enough to minimize temperature fluctuations in the tank. The ratio of the heat capacities of the water (in the tank) to solid PCM was about 3,240. In other words, the thermal capacity of the water tank was three orders of magnitude larger than the PCM in the TES to ensure steady state conditions during all the experiments. Furthermore, there was a Chromalox immersion heater installed in the tank with a temperature control sensor that that ensured the HTF temperature for each charging

process was within 0.5^{o}C of the desired temperature in the water tank. Ice was mixed with the water in the tank to ensure colder water temperatures for the discharging process.

3.3 Thermocouple/TES system calibrations

The thermocouples were first calibrated before insertion into the PCM panels using a previously calibrated Brookfield temperature probe. The probe was used as a reference thermometer to establish the temperature in a jar of water at any given time. After the copper and constantan (thermocouple) wires were soldered together at one end of each thermocouple junction, the wires were tagged for easy identification before calibration. Before the water in the jar was heated, the first measurements were recorded when the reference thermometer reached a steady state temperature for about 5 sec. Then the corresponding temperature readings from the thermocouple wires were recorded with the help of an OMEGA HH509R data acquisition unit. Six random readings of each of the thermocouples were recorded and used for calibration purposes using Excel. Both the reference thermometer (RT) and thermocouple wire (TW) temperature values were graphed and correlated using a linear equation as shown in appendix 2. As it can be seen in appendix 2, all the thermocouple wires had a linear response to temperature. Moreover, the slope values of the calibration curves were more or less the same with R^2 greater than 0.99.

After the experimental set up was completed, a calibration validation experiment was conducted. Several isothermal temperature measurements were taken to verify that

the thermocouple measurements were process independent. With just air surrounding the panels inside the TES, and the PCM in solid phase, temperature measurements at all the locations were recorded using an Agilent 34978-A data acquisition unit. After all the measurements were taken, the time-averaged temperature ($\overline{T_i}$) for the last 10 scans of each thermocouple was determined. Also, the grand time-averaged ($\overline{\overline{T}}$) of all the thermocouple readings were calculated using Excel. The grand average ($\overline{\overline{T}}$) was subtracted from each thermocouple's averaged temperature ($\overline{T_i}$) to determine the correction factor for each thermocouple under isothermal conditions. A similar procedure was repeated with the TES subjected to two separate conditions. For the first condition, 21^{o}C water was pumped through the system for 10 minutes and measurements were taken 2 minutes after the water was drained out from the TES using valve V8. The other condition involved filling the TES with 11^{o}C water while temperature measurements were recorded. For all 3 conditions, the difference between the average thermocouple readings and the grand average readings were within the range of -0.35 to 0.30^{o}C, suggesting that the thermocouples were reliable under varying conditions. Data for all three conditions can be found in appendix 3.

3.4 Experimental procedure

Several experiments were performed to find the temperature distribution within the PCM during melting and solidification processes. Table 4 lists the different experiments performed and their respective conditions. Each experiment consisted

of a charging and discharging runs designated with the letters C and D, respectively as shown in Table 4. Preceding each experiment, cold water at about 19^{o}C was first circulated through a by-pass line to set the flow rate for the experiment with the help of valve V7. When the required flow was attained, valve 6 was closed, valves 1, 3 and 4 were opened (for downward flow) for a substantial amount of time until all the

Table 4. Performed **e**xperiments and conditions

Experiment		**Q $m^3/s \times 10^{-4}$ (GPM)**	**Re No.**	**T_{HTF} (°C)**	**Ste No.**	**Time (s)**	**Flow direction**
1	C	4.03 (6.40)	14,070	32.0	0.029	800	Downward
	D			21.3	-	800	
2	C	4.03 (6.40)	14,070	36.0	0.059	800	
	D	8.25 (13.10)	28,800	20.7	-	800	
3	C	1.54 (2.45)	5,385	32.3	0.029	720	
	D			15.0	-	800	
4	C	4.03 (6.40)	14,070	32.3	0.029	250	Upward
	D			21.5	-	250	

C: charge, D: discharge

thermocouple readings were about 21^{o}C. Temperature data were recorded at time intervals of 10sec. At the end of each run, the water in the TES was drained out using valve 8. Charging and discharging processes of the TES were repeated at different inlet HTF temperatures and mass flow rates in the turbulent range.

Before each charging run, the heater was set to the required temperature, and when the required temperature was attained in the storage tank, the HTF was pumped through the by-pass line while the heater was still on. This was done to ensure that the

HTF temperature was uniform. During the charging experiment, the HTF was pumped through the TES in the direction designated for the experiment under consideration until the PCM temperature was within 1^{o}C of the HTF. For experiment 4, valves 1, 4 and 6 were closed with valves 2, 3, and 5 opened for upward flow through the TES temperature. Before the discharging run, 2 buckets of ice blocks were poured into the tank and stirred to cool it down to a temperature (over 10^{o}C) lower than the melting point temperature of the PCM. Like in the charging run, the HTF was pumped through the by-pass for some time before the valves to the TES unit were opened to initiate the discharge process. The key HTF parameters used for analyzing the experimental results were the Reynolds (Re) and Stefan (Ste) numbers. These parameters were calculated using the following equations:

$$\mathrm{Re} = \frac{4\dot{m}}{\pi \mu D_h} \qquad (3)$$

$$Ste = \frac{c(T_{HTF} - T_m)}{\lambda} \qquad (4)$$

where $\dot{m}$ is the mass flow rate through the system (kg/s), D_h is the hydraulic diameter of the TES (m), μ is the dynamic viscosity of the HTF (Nsm^{-2}), T_{HTF} is the inlet temperature of the heat transfer fluid (^{o}C), T_m is the PCM melting temperature (^{o}C), c is the specific heat (J-kg^{-1}K^{-1}), and λ is the latent heat of fusion of the PCM (kJ/kg). The hydraulic diameter of the devised TES is 4.3 cm (1.7-in). See appendix 5 for the calculation.

3.5 Limitations of the study

Even though the devised experimental set up was designed taking account a variety of operational considerations and conditions, the following constraints had to be taken into account:

- Since reaching a 0°C temperature variation was considered to be impractical given the melting point of the PCM and the ambient conditions, a temperature variation of about 0.7^{o}C within the PCM before the start of each experiment was used to determine if the TES system had reached steady state.
- Only turbulent flow conditions were considered due to the size of the TES, the accuracy of the flow meter, and capacity of the pump.
- Limited standardization of experimental methodologies used by other authors that studied TES systems made it difficult to do a comprehensive comparison among different studies.

CHAPTER IV

RESULTS AND DISCUSSION

4.1 Thermal symmetry validation

First and foremost, the temperature readings at the positions G2 and G3 of panel 4 were compared with their corresponding positions on panel 1 (B2 and B3) as illustrated in Fig. 13. The essence of this was to check for thermal response symmetry within the TES as mentioned earlier.

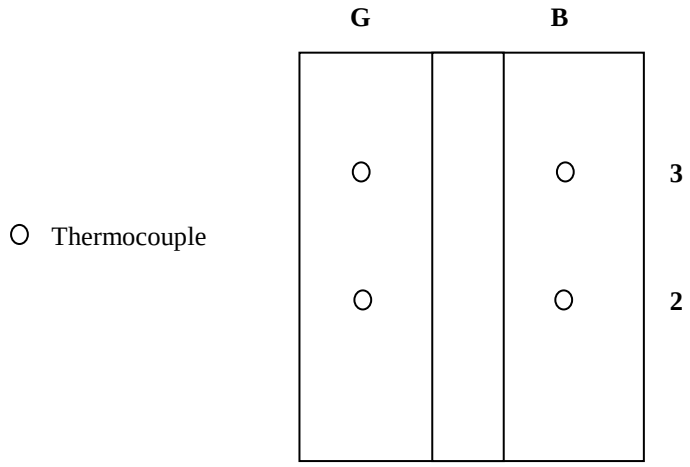

Fig. 13 Validation test thermocouples

Fig. 14 shows the transient temperature profiles for the four considered positions. As observed, there seem to be relatively good agreement between the thermocouple pairs (G2 and B2, G3 and B3) indicating good symmetry within the TES system. Fig. 15 shows the temperature differential between the thermocouple pairs. As can be seen during the latent heating section of the plot (2 through 12 mins), small difference between the thermocouple pairs exist. However, there is more variation within the first two minutes (of sensible heating) which could be attributed to initial temperature

variation as high as 0.7 °C at the different positions before charging started as explained in the previous page.

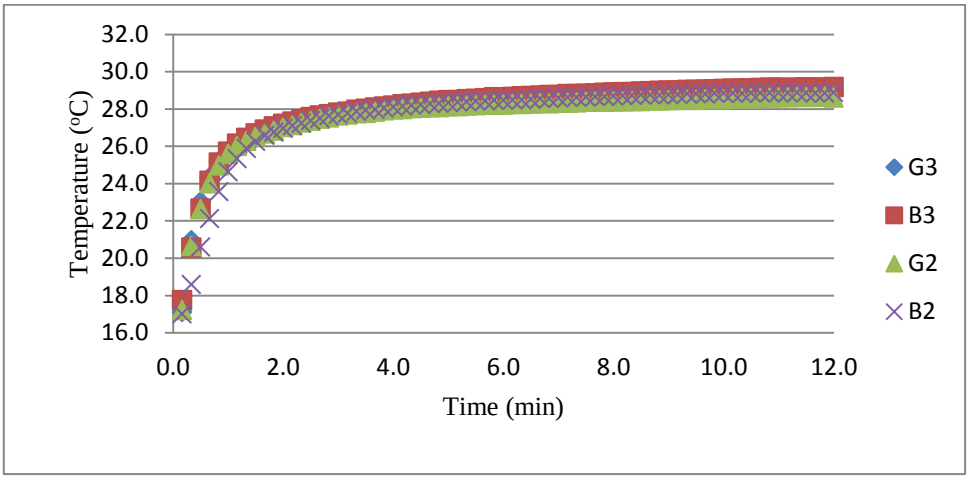

Fig. 14 Temperature profile along channels G and B during charging of experiment 3 [Re = 5,385 downwards, Ste = 0.029, T_{HTF} = 32°C]

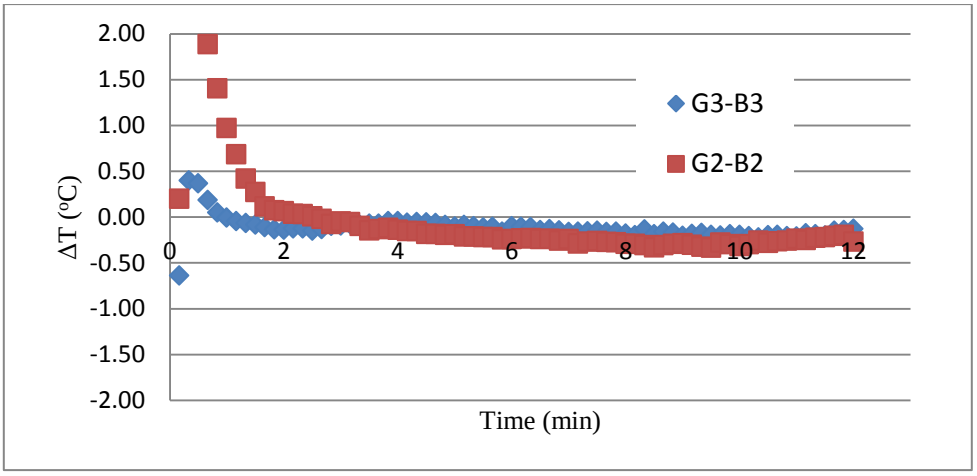

Fig. 15 Temperature differential between channels B and G during charging of experiment 3 [Re = 5,385 downwards, Ste = 0.029, T_{HTF} = 32°C]

4.2 Effect of Stefan's number on charging process

Fig. 16 through 19 show transient temperature plots at different axial locations of interest during the charging process for experiments 1 and 2. Fig. 16 and 17 depict the transient temperature response of the PCM along channels C and E, respectively for a low Stefan number of 0.029. In Fig. 16, at the beginning of the charging process, the heat from the HTF is responsible for the sensible heating of the solid PCM, as seen by the sharp rise of the PCM temperature from 23 to 28^{o}C in about 1.5 min. When the melting point (28^{o}C) was attained, phase change started in the PCM (from about 1.8 min), and subsequent heat addition to the PCM was manifested with relatively little temperature rise compared to the first 1 min of the charging process. Similar trends were

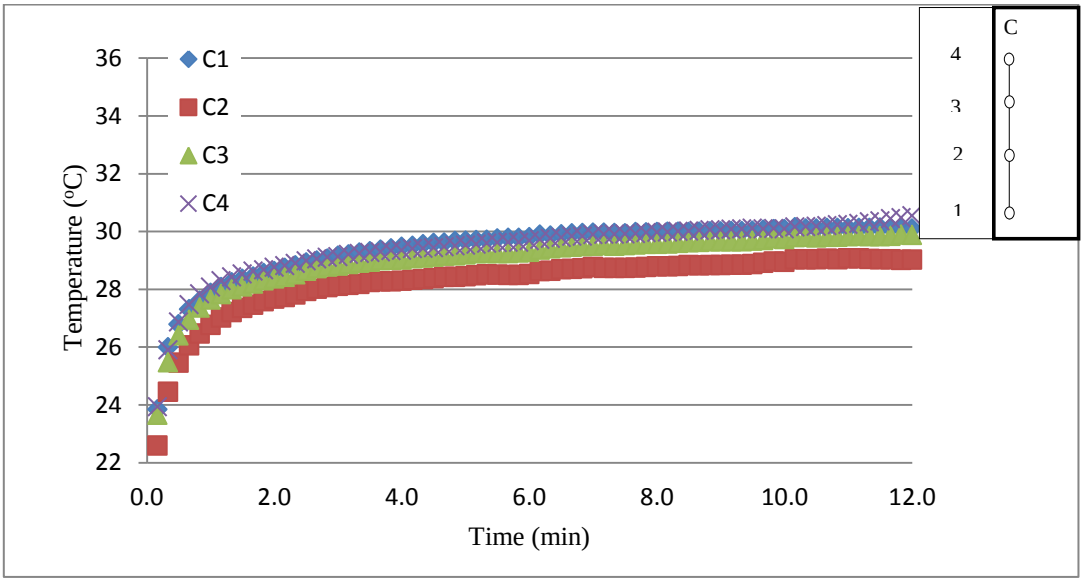

Fig. 16 Temperature profile along channel C during charging of experiment 1 [Re = 14,070 downwards, Ste = 0.029, T_{HTF} = 32^{o}C]

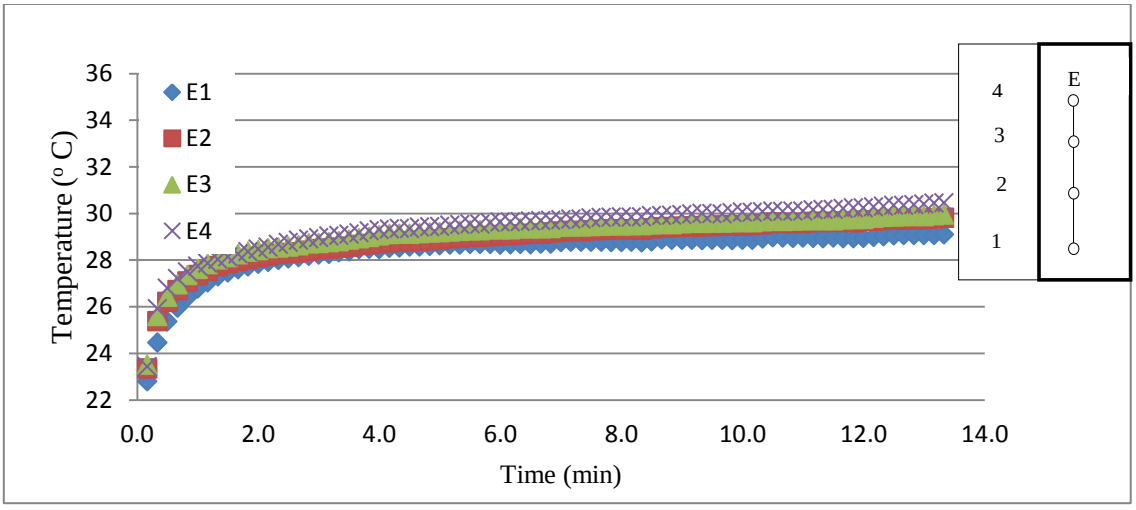

Fig. 17 Temperature profile along channel E during charging of experiment 1 [Re = 14,070 downwards, Ste = 0.029, T_{HTF} = 32°C]

observed along channel E as seen in Fig. 17 above. Another noticeable trend at a low Stefan number is the straightness and monotonic behavior of the profiles (in Fig. 16 and 17) suggesting little or no natural convection effects within the PCM panel. However, it is likely that some convection effects could have happened at intermediate positions between axially adjacent thermocouple locations. Nevertheless, heat conduction was considered to be the relevant heat transport mechanisms at low Stefan number.

Fig. 18 and 19 show the transient thermal response along channels C and A at a Stefan number (higher HTF temperature) of 0.059. As expected, at increased HTF temperature, phase change takes place faster. In Fig. 18, the PCM in channel C attained its melting point at about 60 sec, approximately 35% less than the time observed in experiment 1. As observed in Fig. 18 (and also Fig. 19) between 5 and 11 min, there is a change in thermal response at each thermocouple position. Furthermore, it can be seen that the topmost position experiences phase change sooner than the other three locations

along the same channel. This could be attributed to the fact that the PCMs at those locations are closer to relatively hotter HTF (and heat) by virtue of their position. Another anticipated and important effect of a higher Stefan number is the onset of natural convection. Interestingly, the temperature profile for C2 (Fig. 18) rises sharply when compared to C1 at 10 min. This suggests the onset of buoyancy drives the molten PCM upwards (towards C2) while the denser PCM falls towards C1. External forced convection had a marked effect on C1 since it experienced different thermal response than C2.

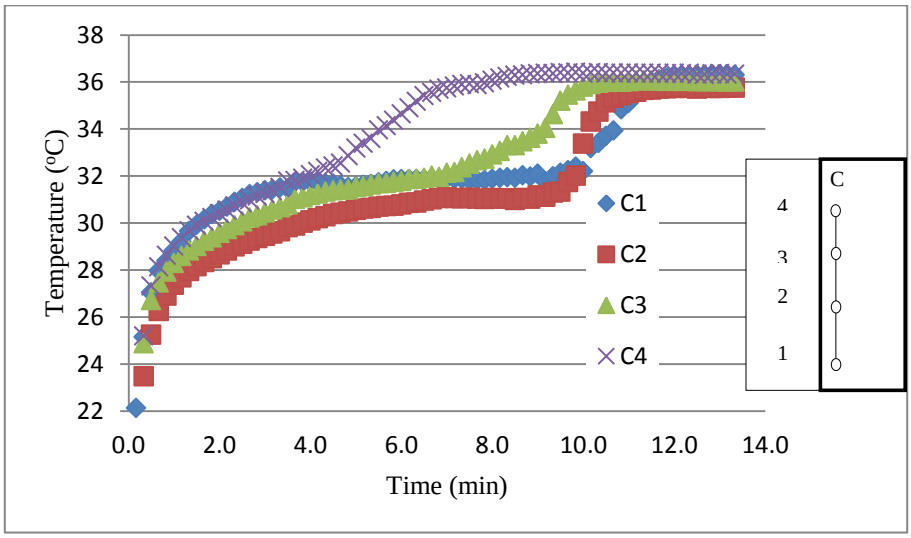

Fig. 18 Temperature profile along channel C during charging of experiment 2 [Re = 14,070 downwards, Ste = 0.059, T_{HTF} = 36°C]

Fig. 19 shows the temperature profile along channel A at the same Stefan number of 0.059. The plot is characterized by temperature drops along the profile of positions A1 and A2 between 4 and 10 min. Typically, at the bottom surface of panel 1, there is a forced convection effect from the HTF which enhances phase change in the PCM at the

lower region compared to intermediate positions such as A2 and A3. So when melting starts at sites lower than A1, colder and denser PCM at A1 drops down while the hotter and lighter melts drift upward. This explains the first temperature drop experienced at about 5 min. When such type of recirculation effect takes place between two axially adjacent thermocouple locations, the higher thermocouple experiences a spike in temperature while the lower one experiences a drop in temperature. Additional sensible

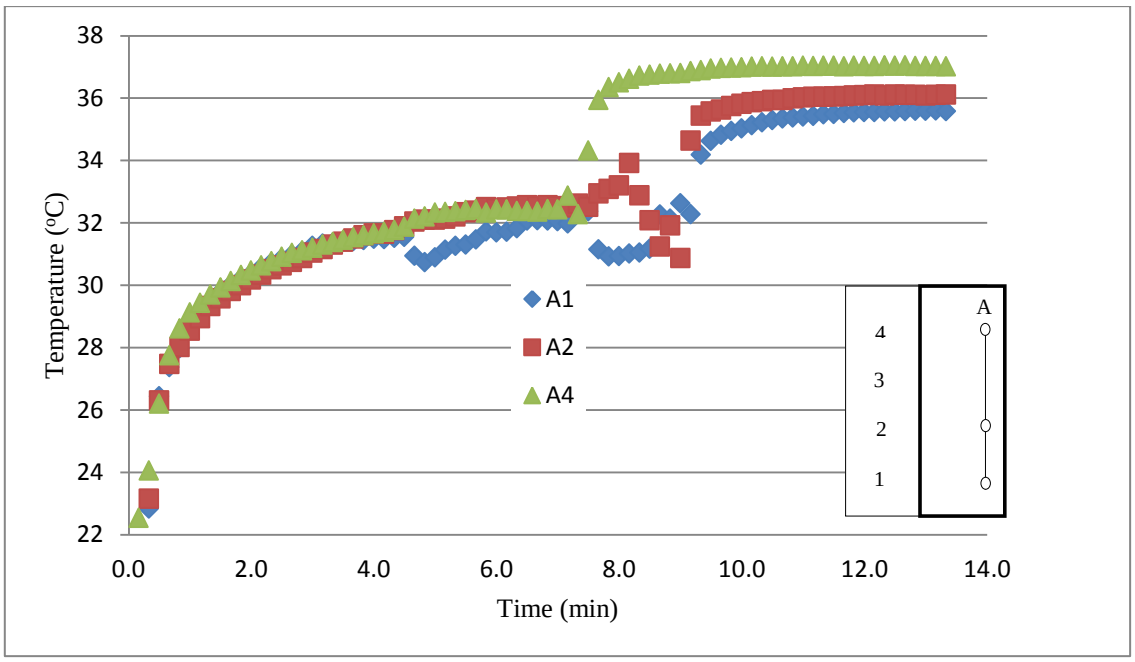

Fig. 19 Temperature profile along channel A during charging of experiment 2 [Re = 14,070 downwards, Ste = 0.059, T_{HTF} = 36°C]

heat addition causes further melting of the cooler PCM, causing an increase in temperature until the molten PCM almost attains the temperature of the HTF. This phenomenon explains the trend seen in profiles of A1 and A2 in Fig.19. At about 7 min when A2 starts experiencing a temperature spike, A1 experiences a temperature drop.

However, the temperature profiles for the top most thermocouples did not experience such temperature drops, as was observed in Fig. 18. Also PCM in the top-most layers melts first before PCM around locations A4, B4 and C4. Thus the density of PCM at the topmost layers is less than at lower regions like A4, B4 and C4. This results in less buoyancy-induced recirculation, which explains why the temperature profiles of C4 and A4 experience no significant temperature drops.

Another important observation was the thermal response of PCM along channel A compared to the others. Fig. 20 shows the transient thermal response profile for the PCM in the radial direction on row 2 for experiment 2. PCMs along channel A were the first to experience buoyancy effects because channel A is located farthest from the center of the TES unit, and thus it has the most interaction with the HTF. Therefore, they

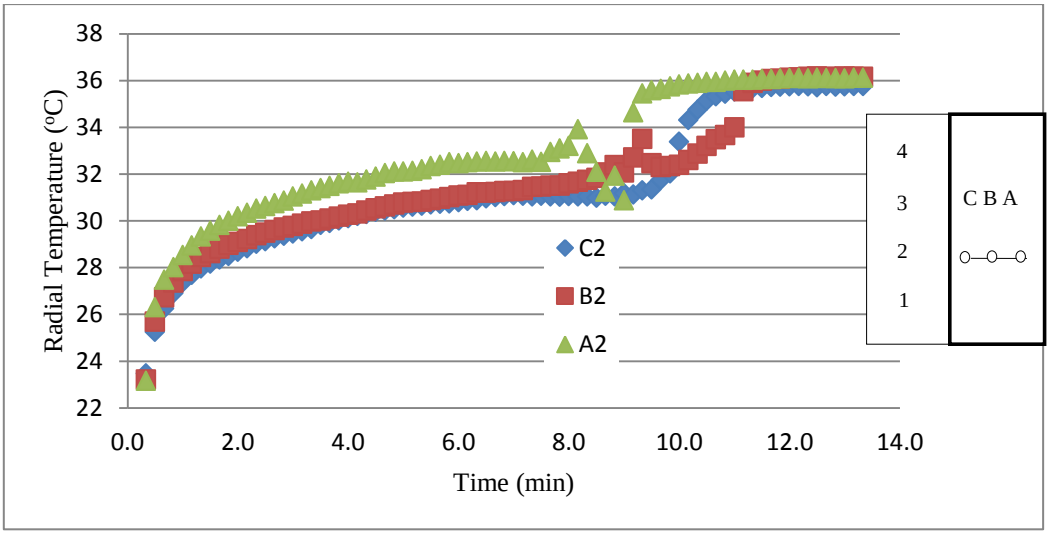

Fig. 20 Transient temperature profiles along row 2 for experiment 2 [Re = 14,070 downwards, Ste = 0.059, T_{HTF} = 36°C]

experience a steep rise in temperature compared to the others. This explains why A2 responded faster than the others at the same radial level as noticed in Fig. 20.

Generally, a buoyancy (density gradient driven) effect is responsible for any drop in temperature observed at any thermocouple positions during the melting, helping to speed up the charging process.

4.3 Effect of Stefan's number on temperature gradients during charging

Vital parameters that should be taken into consideration in the analysis of TES systems are the temperature gradients within the TES during the charging process. Fig. 21 depicts the temperature gradients in the axial direction along channel C. It may also be used to visualize the transient temperature difference between PCM at positions C3 and C2. As observed at a higher Stefan number, the temperature difference for the first six minutes is almost constant. After then, it increases sharply indicating buoyancy driven recirculation effects taking place. It rises to 60^{o}C/cm at about 10 min and starts descending to the zero line indicating the completion of the phase change process at both sites. Similar trends were observed between both rows (2 and 3) along the other channels. Therefore, higher Stefan number has a greater effect on the axial temperature gradient than the low Stefan number. The higher Stefan number results in greater temperature (and density) gradients which aids the melting process through natural convection.

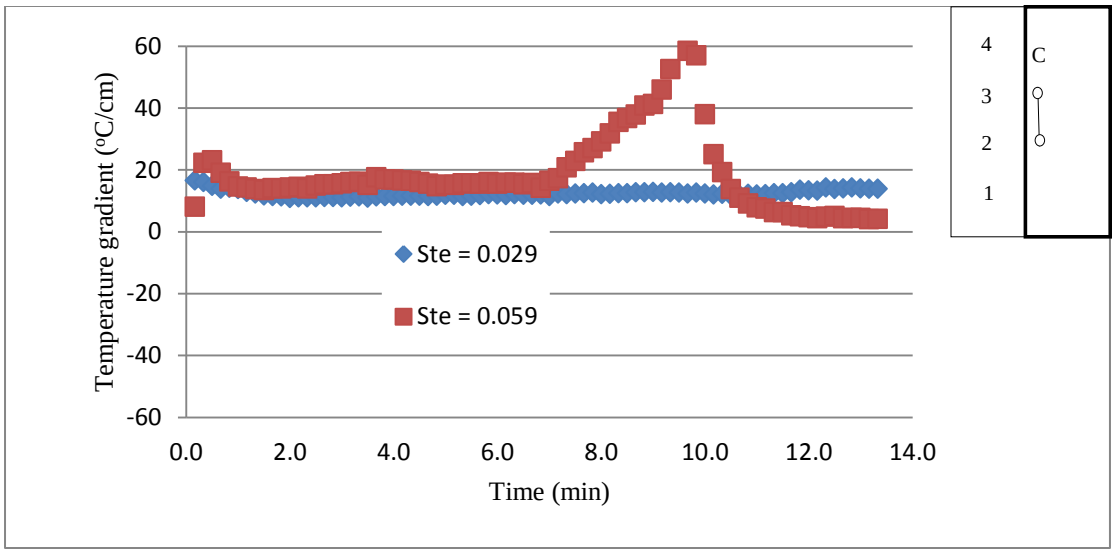

Fig. 21 Axial temperature variation between positions C2 and C3 (i.e. C3 – C2) during charging of experiments 1 (Ste = 0.029) and 2 (Ste =0.059)

Fig. 22 depicts the temperature gradients in the radial direction on row 2 between channels B and C. At a higher Stefan number, higher magnitudes in temperature gradient were observed in the radial direction which also enhanced melting. Again at higher Stefan number, the influence was mainly in the sensible heat part of the melted PCM during charging. As seen, at the higher Stefan number, there was a change in the direction of the temperature gradient just before 10 mins had elapsed. The switch from the positive to negative suggests that the buoyancy effects along channel C intensified and surpassed that of channel B causing uneven sensible heat gain of molten PCM between both channels. Channel B later experienced an intensified buoyancy effect which explains why the profile changed direction just after 10 min.

Although the influence of a higher Stefan number (i.e. higher HTF temperature) is more in the radial direction, the observed trends in Fig. 21 suggest that Stefan number

also has significant effect in the axial direction. Agyenim et al. [54] ran similar experiments using concentric pipes. However, they only observed significant temperature gradients in the radial direction. In the devised TES, the authors were able to achieve significant radial temperature gradients as well as axial gradients which enhanced the phase change process.

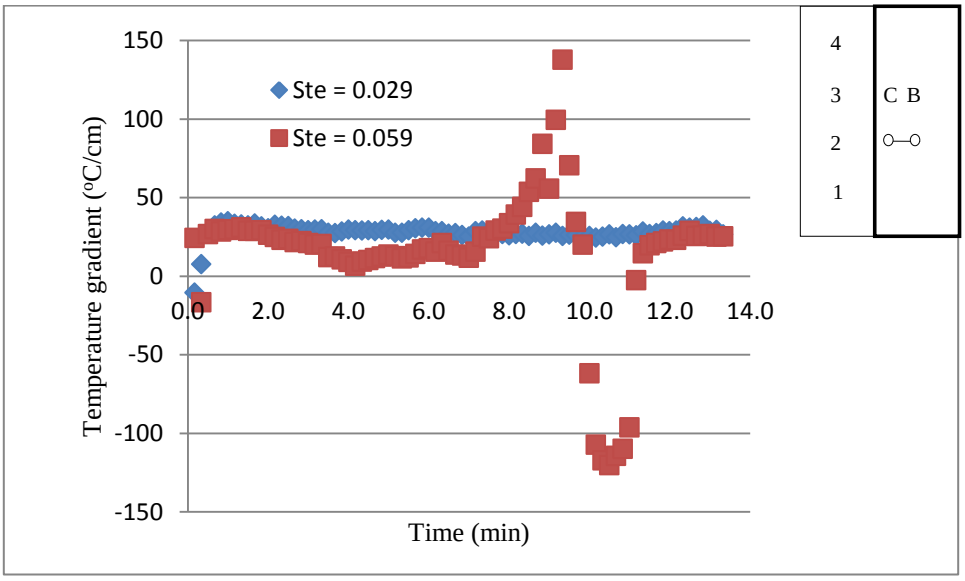

Fig. 22 Radial temperature variation between positions B2 and C2 (i.e. B2 – C2) during charging of experiments 1 (Ste = 0.029) and 2 (Ste = 0.059)

4.4 Effect of Reynolds number on charging process

Fig. 23 and 24 show the transient temperature response of the PCM along the two channels of interest (C and E). Results of the experiments 1 and 3 have been used for comparison purposes. Both had similar Stefan numbers but different Reynolds numbers. Fig. 23 shows the temperature variation along channel E for the charging process of experiment 3. As observed, temperatures at E1, E2 and E3 were lower than that of E4.

For E4, phase change started at about 1.4 min (about 3 min earlier than the others). This was expected due to its proximity to the HTF entering the TES. Temperature profiles for the lower three positions almost merge into one single profile compared to the higher Reynolds number case. For the higher Reynolds number case, there was less separation of the temperature lines between E4 and the other lines suggesting that external convection had a positive effect on the melting process.

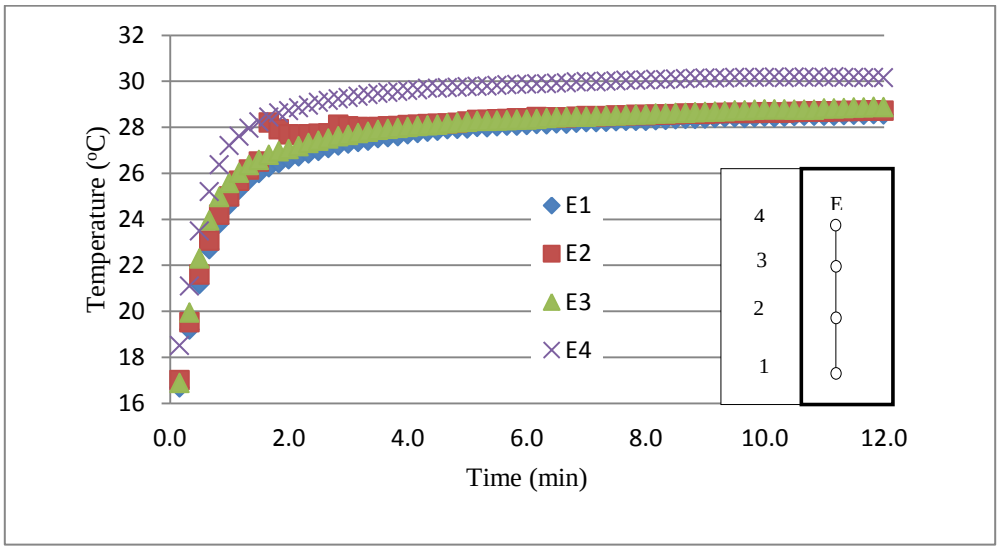

Fig. 23 Temperature profile along channel E during charging of experiment 3 [Re = 5,385 downwards, Ste = 0.029, T_{HTF} = 32°C]

For instance, at a Reynolds number of 14,070, it took position E4 about 1.3 min to start melting and about 2.7 minutes for the lower three positions (see Fig.17) to undergo phase change resulting in a reduction in phase change start time of about 30%. Similar trends and enhancements were observed in the other channels including channel C whose plot is shown in Fig. 24. For the conditions under which the two experiments (1C

and 3C) were performed, natural convection effects could not be observed by merely looking at the plots; however, a combination of natural convection and heat conduction (conjugate problem) could have taken place since a reduction in the time for initiation of phase change was observed.

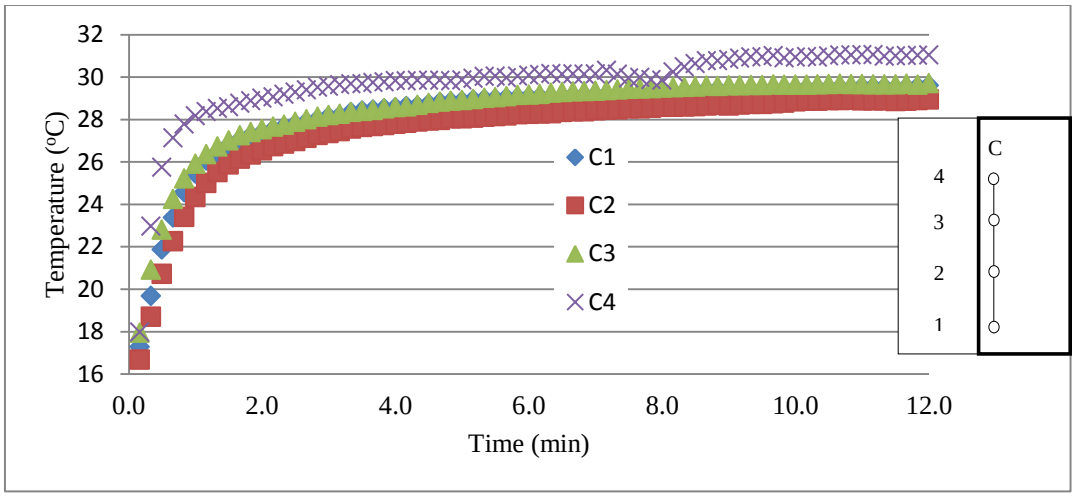

Fig. 24 Temperature profile along channel C during charging for experiment 3 [Re = 5,385 downwards, Ste = 0.029, T_{HTF} = 32°C]

4.5 Effect of Reynolds number on temperature gradients during charging

The effect of Reynolds number on the axial and radial directions of the TES was also examined. Fig. 25 shows the radial temperature gradients on row 2 between channels B and C. It shows the temperature gradients that exist between B2 and C2 for experiments 1 and 3. As observed, a greater temperature gradient was achieved in the radial direction at higher Reynolds number. It is also observed that the gradients at the higher Reynolds number maintained a value between 25 and 35°C/cm as opposed to that

of Fig. 22 that experienced a change in temperature gradient from positive to negative at the higher Stefan number. This suggests again, the significance of a high Stefan number in the melting mechanism of the charging process. At a lower Reynolds number, the temperature gradients were also significant for the first 3 min but declined rapidly as seen below. However, the fall of the temperature gradient at lower Reynolds number

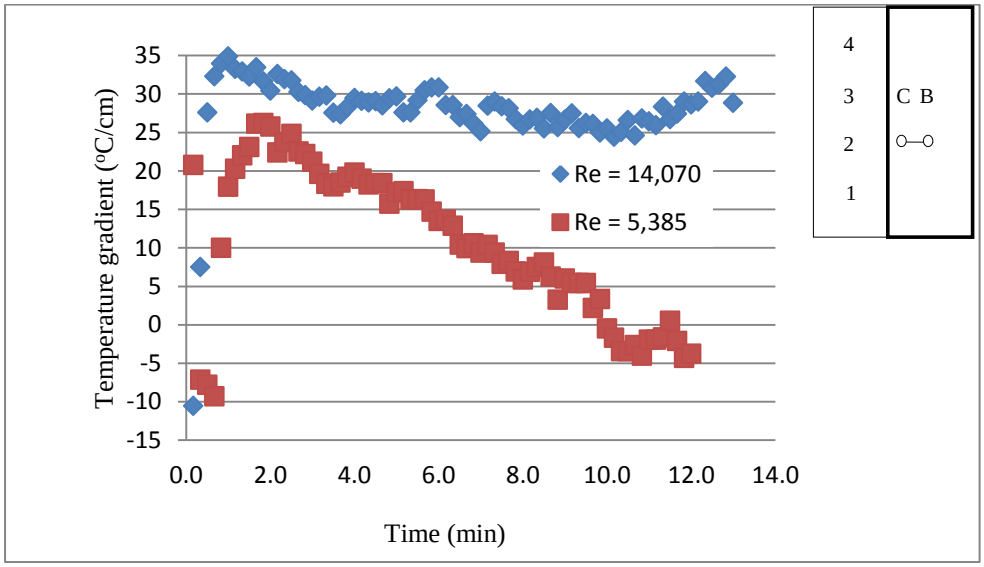

Fig. 25 Radial temperature variation between positions B2 and C2 (i.e. B2 – C2) of experiments 1 (Re = 14,070) and 3 (Re = 5,385) during charging

suggests that internal natural convection effects have a bigger role in the melting process.

Fig. 26 shows the axial temperature gradients on channel C between rows 2 and 3. It shows the temperature gradients that exist between C3 and C2 for experiments 1 and 3. The influence of a higher Reynolds number on the axial direction was

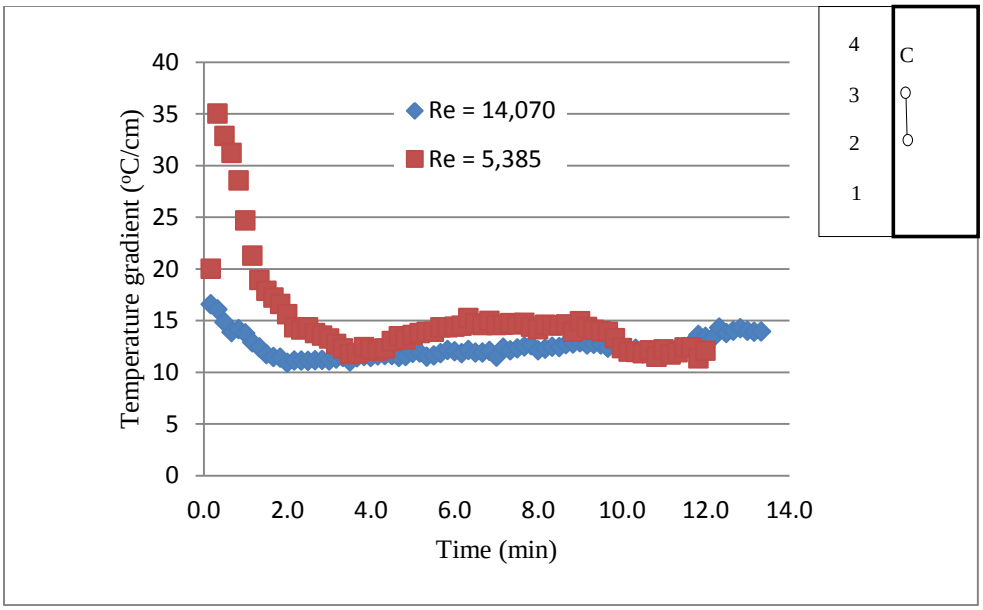

Fig. 26 Axial temperature variation between positions C2 and C3 (i.e. C3 - C2) of experiments 1 (Re = 14,070) and 3 (Re = 5,385) during charging

significant only at initial stages of melting as seen above. After the melting temperature was attained, the gradients remained fairly constant between 10 and 15^{o}C/cm. An important observation in the figure above is that at a higher Reynolds number, the magnitude in the temperature gradients for the positions under consideration is lower than that at a lower Reynolds number. The relatively constant gradient at higher Reynolds number results in more steady heat dissipation within the PCM thermal mass. The trends in Fig. 25 and Fig. 26 suggest that Reynolds number (external forced convection) had a significant effect in the radial direction; however, it did not have a significant effect on the axial temperature gradient. Fig. 27 shows the temperature gradients that exist between A2 and A1 for experiments 1 and 3. As seen, the gradients remained positive throughout the test. Moreover, it varied more in channel A compared to C (of Fig. 26). The reason for this behavior is because channel A is farthest from the

TES center which has more interaction with the HTF and relatively lower PCM distribution within the TES. Given the fact that at higher Reynolds number implies greater pressure drop, it makes more sense to use lower Reynolds number to induce phase change within the TES unit.

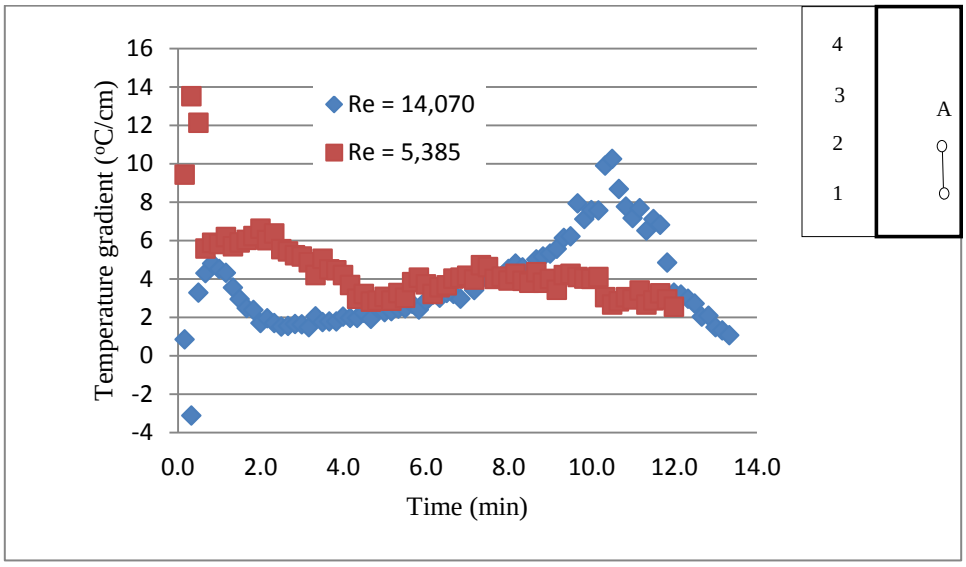

Fig. 27 Axial temperature variation between positions A2 and A1 (i.e. A2 – A1) during charging of experiments 1 (Re = 14,070) and 3 (Re = 5,385)

4.6 Effect of HTF flow direction on the charging and discharging process

The effect of flowing HTF in opposite directions (upwards or downwards) was also considered in this study. The following subsections describe the effect of flow direction on TES performance.

4.6.1 Charging process

For HTF flow in the upward direction, it is anticipated that the buoyancy effects are enhanced compared to downward fluid flow. Since the PCM at the bottom of the TES unit experiences phase change first during upward HTF flow, buoyancy effects should set in and proceed upward easily.

Fig. 28 shows the temperature response along channel C when the HTF direction was upward. Normally, it will be expected that the temperature profiles align with their respective positions. As observed in Fig. 28, the temperature profiles at C3 and C4 where similar and positioned between the profiles of C1 and C2. This can be attributed to the presence of natural convection (enhanced by forced convection) in the melting process. With regards to charging time, all the positions along channel C attained the

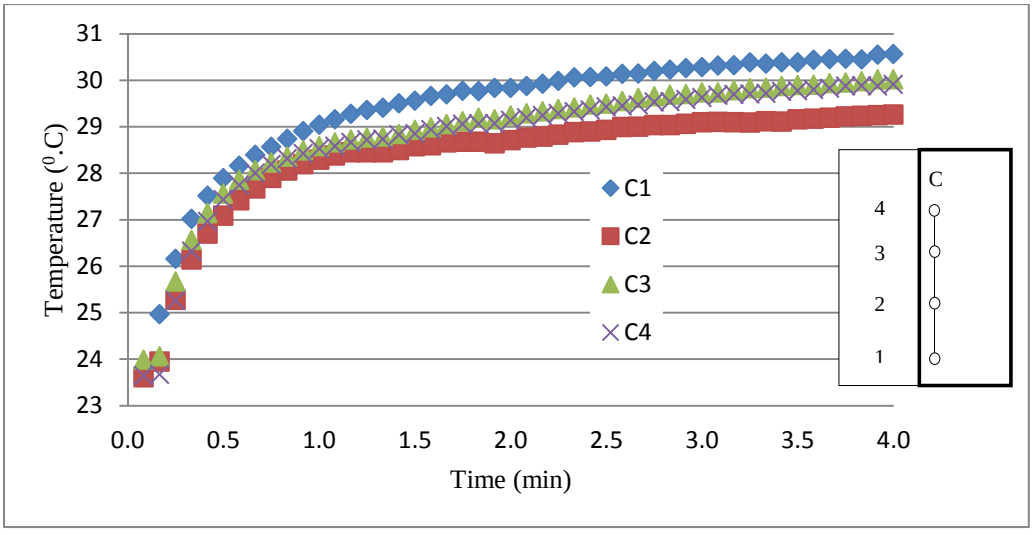

Fig. 28 Temperature profile along channel C during charging of experiment 4 [Re = 14,070 upwards, Ste = 0.029, T_{HTF} = 32^{o}C]

melting temperature at about 0.8 min (50 sec) which represents about 70% reduction in charging time compared to the charging process of experiment 1.

Fig. 29 shows the temperature response along channel B. It is very similar to Fig. 28 for channel C. Though the profiles in Figs. 28 and 29 do not exhibit temperature drops, the authors believe that at a higher Stefan number, such features may be likely.

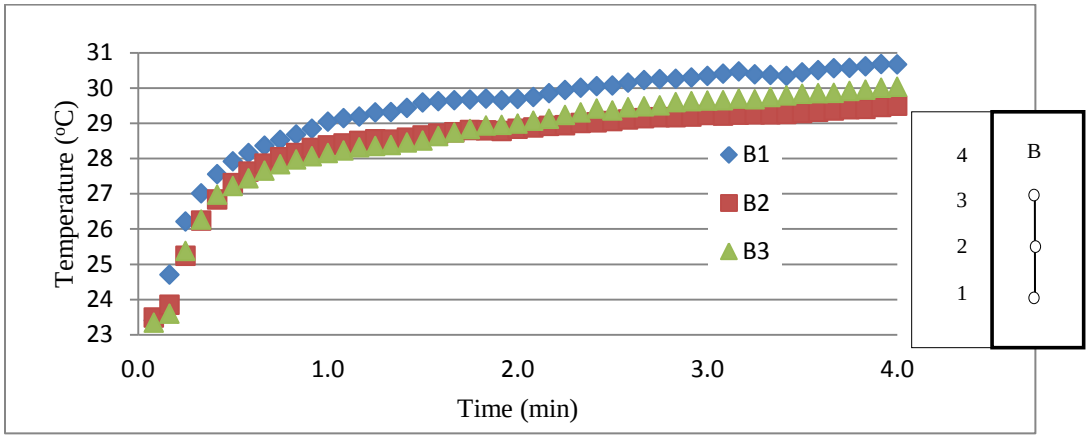

Fig. 29 Temperature profile along channel B during charging of experiment 4 [Re = 14,070 upwards, Ste = 0.029, T_{HTF} = 32°C]

4.6.2 Discharging process

Fig. 30 through 32 shows typical temperature transients during the discharging process (solidification) along channel C under different conditions. Initially, the process starts with the PCM being in the molten state. At a sufficiently high PCM temperature (about 5°C above its melting point), with HTF flowing at a low temperature (about 8°C below the melting point) and high mass flow rate, it is expected to see a sharp decline in PCM temperature. Fig. 30 confirms this expectation. The conditions include a very high Reynolds number of 28,800, discharge HTF temperature of 22.7°C, and an initial

average PCM temperature of 34^{o}C. The high Reynolds and a high temperature difference of about 14^{o}C account for the steep decline in temperature observed within the first 2 minutes of the process. After the melting point was reached, a gradual temperature change followed until the temperature difference between the PCM and HTF was about 0.5^{o}C. However, other discharging experiments did not exhibit a steep decline in PCM temperature. The reason attributed to this observation is the low temperature difference between the final charging temperature of the PCM and the melting point (i.e. low temperature difference leads to lower heat transfer).

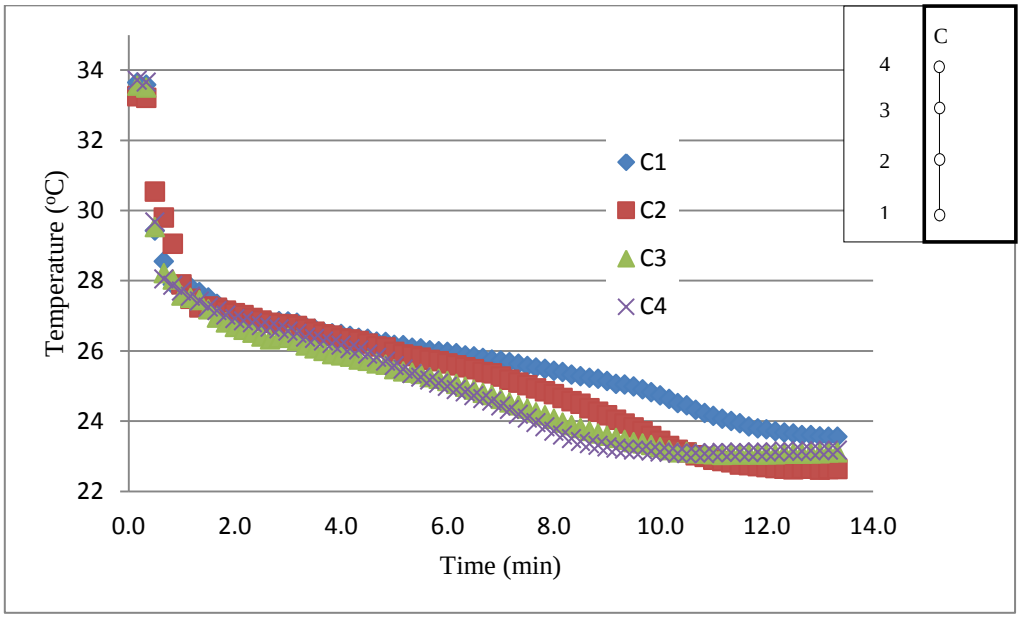

Fig. 30 Temperature profile along channel C during discharging of experiment 2 [Re = 28,800 downwards, T_{HTF} = 22.7^{o}C]

Fig. 31 shows the transient temperature profile along channel C in experiment 1. As seen, the discharging process started at about 28^{o}C and declined gradually to the HTF

temperature. Since the HTF flow direction was downward, solidification started at the top (C4) and progressed downward with C1 (the lowest position) being the last to achieve complete solidification. Moreover, the Reynolds number is believed to have a significant effect on the thermal response during solidification which could explain why the profiles in Fig. 30 are relatively closer compared to those in Fig. 31.

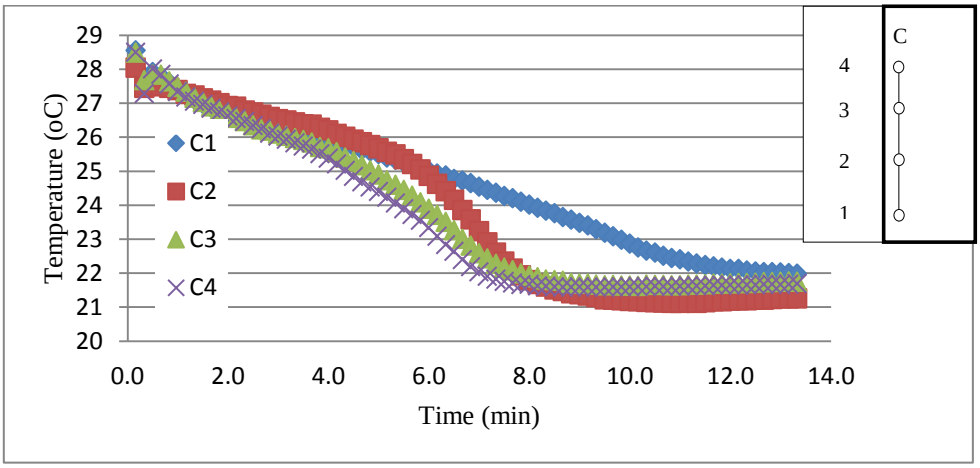

Fig. 31 Temperature profile along channel C during discharging of experiment 1 [Re = 14,070 downwards, T_{HTF} = 21.7^{o}C]

Fig. 32 shows the transient temperature profile along channel E in a similar experiment with the same HTF conditions but with the HTF flowing upwards. As expected, the lowest position experienced solidification first before the rest. It can be estimated from Fig. 32 that all the positions experience complete solidification in about 5 min as opposed to the downward flow condition which took about 12 minutes for complete solidification as seen in Fig. 31. Also, an important observation is the alignment of the temperature profiles in the direction of the HTF (see Figs. 30 through

32). Although natural convection is believed to be present in the liquid PCM at early stages of the discharging process, it tends to diminish rapidly as the solidification progresses and the process becomes conduction-limited. This is evident in Fig. 32 where position E1 undergoes solidification first, while the others lagged slowly behind between 1.6 and 3.6 min.

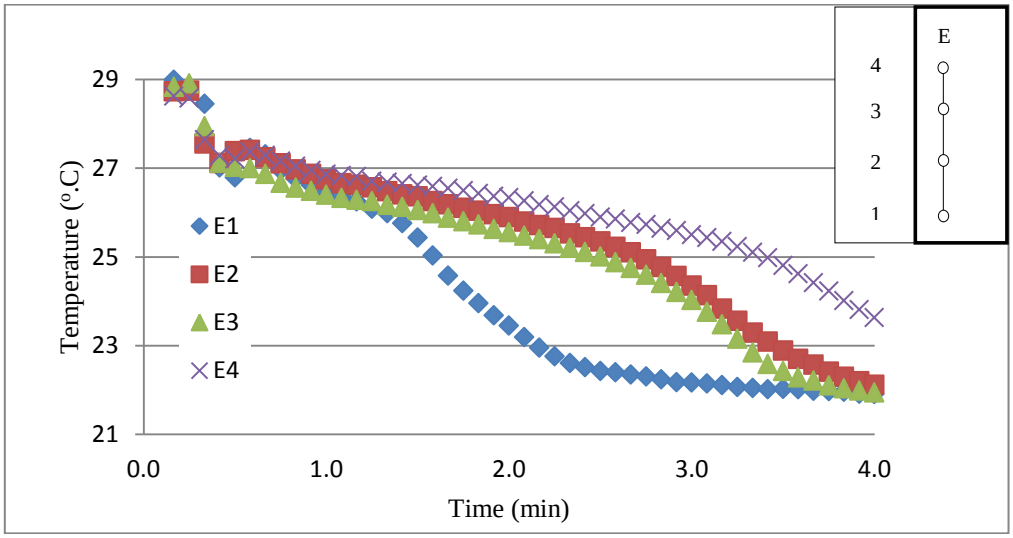

Fig. 32 Temperature profile along channel E during discharging of experiment 4 [Re = 14,070 upwards, T_{HTF} = 21.5°C]

4.7 Comparison of the present system with previous study

Experiment 3 was designed and run for comparison purposes. Estimated experimental conditions similar to those used in [54] were applied to the devised TES in order to make a fair comparison between its performance and that of the multi-tube system proposed by Agyenim et al. [54]. Data from the solid phase sensible heat part of Fig. 13 in [54] during the charging process was used to determine HTF flow conditions

required for comparison purposes (see Fig. 13 in [54] and calculations in appendix 4). Equation 5 was used to proportionally determine the amount of heat required during the charging process of experiment 3 for the devised TES.

$$\frac{\dot{Q}_{[54]}}{(m\lambda)_{[54]}} = \frac{\dot{Q}_{TES}}{(m\lambda)_{TES}} \qquad (5)$$

where $\dot{Q}_{[54]}$ is the sensible heat of the solid PCM from [54], $(m\lambda)_{[54]}$ is the product of the mass (kg) and the latent heat of fusion (kJ/kg) of the PCM used in [54], $\dot{Q}_{TES}$ is the amount of heat required for the designed TES and also is unknown, and $(m\lambda)_{TES}$ is the product of the mass (kg) and the latent heat of fusion for octadecane used in the designed TES (kJ/kg). The parameter $\dot{Q}_{[54]}$ in (5) is equivalent to

$$\dot{Q}_{[54]} = (m\lambda)_{[54]} \times \frac{T_{melt.pt} - T_{inital}}{\Delta t} \qquad (6)$$

where m is the mass of PCM used in the multi-tube of [54], c is the specific heat (kJ-kg^{-1}K^{-1}), and $T_{melt.pt}$ is the melting point temperature (^{o}C) of the PCM used in [54], $T_{initial}$ is the initial temperature of the PCM before charging, and Δt is the time (in sec) required in heating the PCM from the initial solid state to the melting point. All these parameters but $(mc)_{[54]}$ were obtained using the sensible heating part of the charging process in Fig. 13 of [54] as described in appendix 4. So with the result of (6), $\dot{Q}_{TES}$ was obtained in (5) from which the required HTF flow rate was estimated to be about of 7.57 l/min (2 GPM) using equation (7).

$$\dot{Q}_{TES} = (\dot{m}c)_{TES} \times (T_{inlet} - T_{outlet}) \quad (7)$$

where $(\dot{m}c)_{TES}$ is the product of the HTF mass flow rate (kg/s) and the specific heat capacity of water (kJ-kg^{-1}K^{-1}), while T_{inlet} and T_{outlet} are the inlet and outlet temperatures of the HTF, respectively. A ΔT of 0.8°C was used in experiment 3. However, a flow rate of 9.27 l/min (2.45 GPM, Re = 5,385) was used with some valve adjustments to ensure the TES was completely filled with water. A typical transient temperature profile along a channel is shown in Fig. 23. The average slope of the temperature profile in the sensible heat portion of Fig. 23 is 0.13^{o}C/s. The slope of the sensible heat portion of Fig.13 in [54] is about 0.014°C/sec, or about 9 times smaller than the slope of Fig. 23. Even though the thermal load applied in experiment 3 was proportionally about 25% greater than the heat load depicted in Fig.13 of [54], it is evident that the devised TES is relatively faster than the system used in [54].

Fig. 33 shows the transient temperature profile along channel E during the discharging process. It was observed that it took about 11.7 min for the PCMs at all four positions to attain a temperature of 16^{o}C. Thus, for the devised TES, the discharging time was about 40% greater than the charging time in experiment 3. In [54], the discharging time was estimated (from Fig. 13 in [54]) to be about 250% more than that for charging time. This leads to the conclusion that the devised TES can respond faster to charging and discharging conditions.

Though it is understood that the lower charging and discharging times observed in the tested TES compared to the multi-tube of [54] is influenced by the amount of

PCM used (as can be inferred from equation 5), the authors strongly believe that similar behavior should be seen at larger scales if the same configuration is used. At larger scales, lower charging and discharging times are expected because of the high surface area-to-volume ratio of the devised configuration which should result in significant temperature gradients in the radial and axial directions as seen in this study. In Fig. 8 of [54], the axial temperature gradient was insignificant compared to that of the radial; however, by using radially-aligned vertical channels, radial temperature gradients can be as dominant as axial temperature gradients.

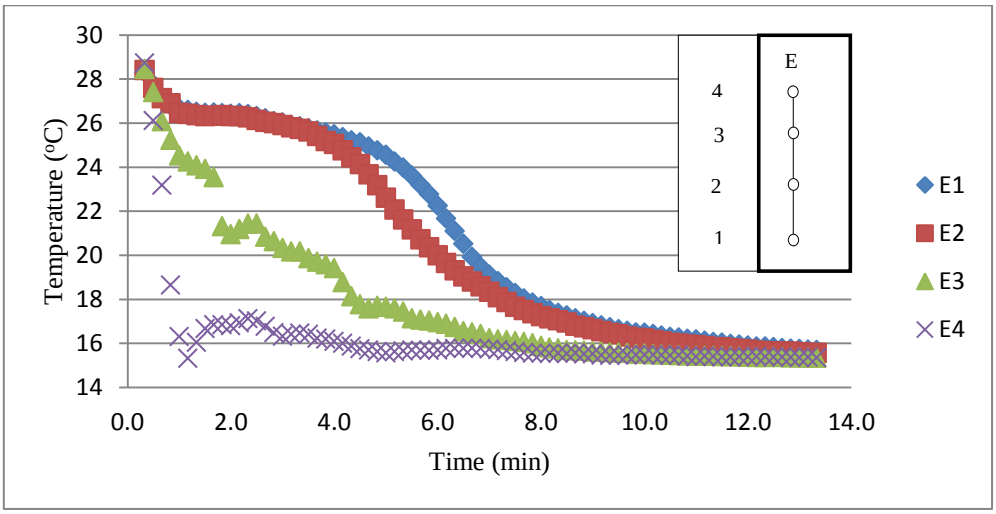

Fig. 33 Temperature profile along channel E during discharging of experiment 3 [Re = 5,385 downwards, T_{HTF} = 15°C]

4.8 Time constant estimates

To quantify the speed of charging and discharging processes under different experimental conditions in a non-dimensional way, the time-dependent temperature data

was non-dimensionalized and fitted to a mathematical model. The following model has been used in the past to fit time-dependent data (Alvarado and Martinez [56]). It was used fit the data of experiments 1 and 4.

$$\theta = e^{-b/t} \tag{8}$$

$$\theta = \frac{T(t) - T(i)}{T(f) - T(i)} \tag{9}$$

where, t, b, T(t), T(i), and T(f) are time in sec, time constant in sec, PCM temperature at time t , initial temperature of PCM, and final PCM temperature respectively. The valid conditions for Equation 8 are that at time t = 0, θ is equal to 0, and as t tends to infinity, θ tends to 1. With this model, the temperature along the considered channels can be estimated if time is known.

In the TES, C2 and B2 were considered to be among the last locations where melting occurred during the charging process of experiment 1 (see Fig. 10 on page 39 for these positions). This judgment was made based on the findings from Fig. 34 which shows the axial temperature gradients between the first two horizontal rows of channels A, B and C. The same figure can be used to examine the temperature variations between (A2-A1), (B2-B1) and (C2-C1). As can be seen, the temperature gradients of channels B and C exhibit large negative values compared to channel A where the temperature gradients are positive with HTF flow in the downward direction. Similar trends were observed in all other charging experiments between rows 1 and 2, including the charging process of experiment 4 with upward flow of HTF. With this in mind, the model proposed above has been applied to points C2 and B2 for experiments 1 (downward flow

of the HTF) and 4 (upward flow of the HTF). Equation 9 was used to fit the temperature data for points B2 and C2, to determine the response speed of these positions in two flow directions. Table 5 shows the corresponding fitted equations for the two cases considered.

As seen in Table 5, flow direction plays a decisive role on how fast or slow the charging process takes. By flowing the HTF upwardly, the thermal speed of the phase change process almost doubled as captured by a decrease in the value of b by a factor of about 2. This confirms several of the observations stated above including the fact that induced natural convection enhances the phase change process within each TES channel.

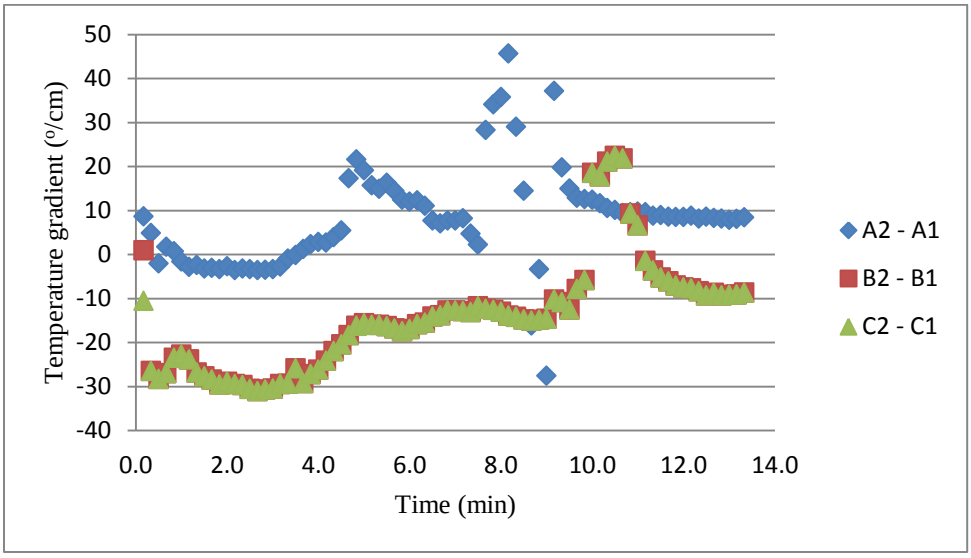

Fig. 34 Axial temperature variation between rows 1 and 2 during the charging process of experiment 2 [Re = 14,070 downward, Ste = 0.059, T_{HTF} = 36°C]

Table 5. Time constants for charging process

Experiment	Position	Fitted equation (9)	R^2	Response time parameter (b)
1: Re = 14,070 Ste = 0.029 downward flow, Charging	B2	$\theta = e^{-0.48/t}$	0.96	0.48
	C2	$\theta = e^{-0.56/t}$	0.97	0.56
4: Re = 14,070 Ste = 0.029 upward flow, Charging	B2	$\theta = e^{-0.24/t}$	0.98	0.24
	C2	$\theta = e^{-0.26/t}$	0.98	0.26

CHAPTER V

CONCLUSIONS

An experimental investigation has been conducted to study the thermal performance of octadecane as a PCM in a TES system incorporating corrugated copper panels. The data suggest that the devised TES is more effective than the multi-tube system proposed by Agyenim et al. [54] due to the reduction in discharging and charging times. The significant enhancement is attributed to the characteristic higher surface area-to-volume ratio of the devised TES.

Of the two main parameters, Reynolds and Stefan numbers, the thermal response of the TES is more sensitive to Stefan number variation than to Reynolds number. Furthermore, very significant buoyancy effects can be detected at higher HTF temperatures which seemed to have aided the phase change process. As observed, an increase in the HTF inlet temperature resulted in higher radial and axial temperature gradients throughout the TES as opposed to the multi-tube system. Considering flow direction of the HTF, buoyancy effects did play a significant role in increasing the speed of the phase change process. Furthermore, there were significant reductions in charging and discharging times which can be attributed to natural convection and the direction of HTF. Basically, optimum performance of the devised TES can be achieved by taking advantage of HTF temperatures and flow direction.

5.1 Future Work

A majority of the studies undertaken on phase change materials have reported poor thermal conductivities requiring heat transfer enhancement. There are no national and international standards for testing PCMs. As such, researchers have over the years applied different approaches in both test procedures and analysis of results. The development of a unified international standard for test and analysis will be helpful in the development of latent heat thermal energy storage systems. Also, contradictions still exist in the thermo-physical properties of PCMs provided especially the latent heat of fusion, thermal conductivity and densities in solid and liquid states. This is again due to the absence of unified certification standards and procedures.

Also, a comprehensive parametric investigation using parameters such as Stefan number, Reynolds number, and Raleigh number for both directions of the HTF in the designed TES should be considered.

REFERENCES

[1] T. W. Kerslake, M. B. Ibrahim, Analysis of thermal energy storage material with change-of-phase volumetric effects, ASME Journal of Solar Energy115 (1993) 22–31

[2] G. A. Lane, Solar Heat Storage: Latent Heat Materials, Vol. I, Boca Raton, Florida, CRC Press, 1983.

[3] A. Abhat, Low temperature latent thermal energy storage system: heat storage materials, Solar Energy 30 (1983) 313–332.

[4] M. Telkes, Thermal Storage for Solar Heating and Cooling. In: Proceedings of the Workshop on Solar Energy Storage Sub-systems for the Heating and Cooling of Buildings. University of Virginia, Charlottesville, Virginia; NSF/RANN/75/041, 1975.

[5] X. Wang, E. Lu, W. Lin, T. Liu, Z. Shi, R. Tang, C. Wang, Heat storage performance of the binary systems neopentyl glycol/pentaerythritol and neopentyl glycol/trihydroxy methyl-amino methane as solid-solid phase change materials, Energy Conservation and Management 41 (2000) 129–134.

[6] S.D. Sharma, K. Sagara, Latent heat storage and systems: a review, International Journal of Green Energy 2 (2005) 1–56

[7] F. Agyenim, N. H. Hewitt, P. Eames, M. Smyth, A review of materials, heat transfer and phase change problem formulation for latent heat thermal energy storage systems (LHTESS), Renewable and Sustainable Energy Reviews 14 (2010) 615–628

[8] D. J. Morisson, S. I. Abdel-Khalik, Effects of phase change energy storage on the performance of air based and liquid solar heating systems, Solar Energy 20 (1978) 57–67

[9] D.V. Hale, M.J. Hoover, M.J. O'Neill. Phase Change Materials Hand Book, Report no. HREC- 5183-2LMSC-HREC D225138. Marshal Space Flight Center, Huntsville, Alabama;1971.

[10] H.P. Garg, S.C. Mullick, A. K. Bhargava, Solar Thermal Energy Storage. D. Reidel Publishing Co., 1985.

[11] D. Buddhi, R. L. Sawhney, Proceedings of Thermal Energy Storage and Energy Conversion. School of Energy and Environmental Studies. Devi Ahilya University, Indore, India. February 24–25, 1994.

[12] S. Hiran, A. Suwondo, G. Mansoori, Characterization of alkanes and paraffin waxes for application as phase change energy storage medium, Energy Sources 16 (1994) 117–128.

[13] S. Hasnain, Review on sustainable thermal energy storage technologies. Part I: Heat storage materials and techniques, Energy Conservation and Management 39 (1998) 1127–1138.

[14] K.S. Markley, Fatty Acids, Part 4. John Wiley and Sons, 1967.

[15] R.C. Weast, M. J. Astle, CRC Handbook of Data on Organic Compounds, CRC Press Inc., 1985

[16] P. Kauranen, K. Peippo, P. D. Lund, An organic PCM storage system with adjustable melting temperature, Solar Energy 46 (1991) 275 – 278.

[17] G.A. Lane, Phase change thermal storage materials. In: Hand Book of Thermal Design. C. Guyer, editor, McGraw Hill Book Co, 1989.

[18] D.A. Neeper, Potential benefits of distributed PCM thermal storage. In: Coleman MJ, Proceedings of 14th National Passive Solar Conference. Denver, Colorado; American Solar Energy Society, 1989. p 283–288.

[19] D.A. Neeper, Thermal dynamics of wallboard with latent heat storage, Solar Energy 68 (2000) 393–403.

[20] L. Yeh, Review of heat transfer technologies in electronic equipment, Journal of Electronic Packaging 117 (1996) 333–339.

[21] M. A. Esam, C. H. Amon, Thermal analyses of a PCM thermal control unit for portable electronic devices: experimental and numerical studies. IEEE Transactions on Components and Packaging Technologies, 26 (1) (2003) 116–125.

[22] S. Jegadheswaran, S. D. Pohekar, Performance enhancement in latent heat thermal storage system: A review, Renewable and Sustainable Energy Reviews 13 (2009) 2225–2244.

[23] P. Lamberg, R. Lehtiniemi, A. M. Henell, Numerical and experimental investigation of melting and freezing processes in phase change material storage, International Journal of Thermal Science 43 (2004) 277–287.

[24] U. Stritih, An experimental study of enhanced heat transfer in rectangular PCM storage, International Journal of Heat and Mass Transfer 47 (2004) 2841–2847.

[25] Y. Zhang, Z. Chen, Q. Wang, Q. Wu, Melting in an enclosure with discrete heating at a constant rate, Experimental Thermal and Fluid Sciences 6 (1993) 196–201.

[26] Y. Jellouli, R. Chouikh, A.Guizani, A. Belghith, Numerical study of the moving boundary problem during melting process in a rectangular cavity heated from below, American Journal of Applied Sciences 4 (2007) 251–256.

[27] B. J Jones, B. Sun, S. Krishnan, S. V. Garimella, Experimental and numerical investigation of melting in a cylinder, International Journal of Heat and Mass Transfer 4 (2006) 2724–2738.

[28] M. Akgun, O. Aydin, K. Kaygusuz, Experimental study on melting/solidification characteristics of a paraffin as PCM, Energy Conversion and Management 48 (2007) 669–678.

[29] K.W. Ng, Z. X. Gong, A. S. Mujumdar, Heat transfer in free convection-dominated melting of a phase change material in a horizontal annulus, International Communications in Heat and Mass Transfer 25 (1998) 631–640.

[30] A. G Bathelt, R.Viskanta, W. Leidenfrost, An experimental investigation of natural convection in the melted region around a heated horizontal cylinder, Journal of Fluid Mechanics (Part 2) 90 (1979) 227–239.

[31] A. G Bathelt, R. Viskanta, W. Leidenfrost, Latent heat of fusion energy storage: experiments on heat transfer from cylinder during melting, ASME Journal of Heat Transfer 101 (1979) 453–458.

[32] A. G. Bathelt, R. Viskanta, Heat transfer and interface motion during melting and solidification around a finned heat source/sink, ASME Journal of Heat Transfer 103 (1981) 720–726.

[33] L. S.Yao, F. F. Chen, Effects of natural convection in the melted region around a heated horizontal cylinder, ASME Journal of Heat Transfer 102 (1980) 667–672.

[34] R. M. Abdel-Wahed, J. W. Ramsey, E. M. Sparrow, Photographic study of melting about an embedded horizontal heating cylinder, International Journal of Heat and Mass Transfer 22 (1979) 171–173.

[35] A. F. Regin, S. C. Solanki, J. S. Saini. Latent heat thermal storage using cylindrical capsule: numerical and experimental investigations, Renewable Energy 31 (2006) 2025–2041.

[36] P. A. Bahrami, Natural melting within a spherical shell. NASA Technical Memorandum1990; 102822, Ames Research Center, Moffett Field, California.

[37] F. L. Tan, Constrained and unconstrained melting inside a sphere, International Communication in Heat and Mass Transfer 35 (2008) 466–475.

[38] H. Ettouney, H. El-Dessouky, A. Al-Ali. Heat transfer during phase change of paraffin wax stored in spherical shells, ASME Journal of Solar Energy Engineering 127 (2005) 357–365.

[39] P.G. Kroegar, S. Ostrach, The solution of two-dimensional freezing problem including convection effects in the liquid region, International Journal of Heat Transfer 17 (1973) 1191–1207

[40] H. Ettouney, H. El-Dessouky, E. Al-Kandari, Heat transfer characteristics during melting and solidification of phase change energy storage process, Industrial and Engineering Chemistry Research 43 (2004) 5350–5357.

[41] J. Wang, G. Chen, H. Jiang, Theoretical study on a novel phase change process, International Journal of Energy Research 23 (1999) 287–294.

[42] M. M. Farid, A. Kanzawa, Thermal performance of a heat storage module using PCMs with different melting temperatures: mathematical modeling, ASME Journal of Solar Energy Engineering 111 (1989) 152–157.

[43] H. Michels, R. Pitz-Paal, Cascaded latent heat storage for parabolic trough solar power plants, Solar Energy 81 (2007) 829–837.

[44] J. Wang, G. Chen, F. Zheng, Study on phase change temperature distributions of composite PCMs in thermal energy storage systems, International Journal of Energy Research 23 (1999) 277–285.

[45] R. V. Seeniraj, N. L. Narasimhan, Performance enhancement of a solar dynamic LHTS module having both fins and multiple PCMs, Solar Energy 82 (2008) 535–542.

[46] X. Gong, A. S. Mujumdar, A new solar receiver thermal store for space-based activities using multiple composite phase-change materials, ASME Journal of Solar Energy Engineering 117 (1995) 215–220.

[47] H. Cui, H. Yuan, X. Hou, Thermal performance analysis for a heat receiver using multiple phase change materials, Applied Thermal Engineering 23 (2003) 2353–2361.

[48] F. P Incropera, D. P. Dewitt, T. L. Bergman, A. S. Lavine. Introduction to Heat Transfer. In: One dimensional steady-state conduction. John Wiley and Sons, 2007 p. 96–200.

[49] A. Sharma, V. V. Tyagi, C. R. Chen, D.Buddhi, Review on thermal energy storage with phase change materials and applications, Renewable and Sustainable Energy Reviews 13 (2009) 318–345.

[50] M. Lacroix, Study of the heat transfer behavior of a latent heat thermal energy storage unit with a finned tube, International Journal of Heat and Mass Transfer 36 (1993) 2083–2092.

[51] Y. Zhang, A. Faghri, Heat transfer enhancement in latent heat thermal energy storage system by using an external radial finned tube, Journal of Enhanced Heat Transfer 3 (1996) 119–127.

[52] E. Gundher, H. Mehling, S. Hiebler, Modeling of subcooling and solidification of phase change materials, Modeling and Simulations in Material Science and Engineering 15 (2007) 879–892.

[53] R. V. Seeniraj, R.Velraj, N. L. Narasimhan, Thermal analysis of a finned-tube LHTS module for a solar dynamic power system, Heat and Mass Transfer 38 (2002) 409–417.

[54] F. Agyenim, P. Eames, M. Smith, Heat transfer enhancement in medium temperature thermal storage system using a multi tube heat transfer array, Renewable Energy 35 (2010) 198–207

[55]Y. Shiina, T. Inagaki, Study on the efficiency of effective thermal conductivities on melting characteristics of latent heat storage capsules, International Journal of Heat and Mass Transfer 48 (2005) 373 –383

[56] J. Alvarado, E. Martinez, Passive cooling of cement-based roofs in tropical climates, Energy and Buildings 40 (2008) 358–364

APPENDIX 1

TEMPERATURE DEPENDENT THERMO-PHYSICAL PROPERTIES OF OCTADECANE

Source: National Institute of Standard and Technology (NIST) website: (http://wtt-pro.nist.gov/wtt-pro/index.html?cmp=octadecane)

Table A-1 Thermal conductivity variation with temperature for octadecane

Temperature (^{o}C)	Thermal conductivity, k (W/m-K)	Uncertainty (W/m-K)
40	0.1464	0.0033
41	0.1462	0.0033
43	0.1459	0.0032
45	0.1455	0.0031
47	0.1452	0.0030
49	0.1448	0.0029
51	0.1445	0.0028
53	0.1441	0.0027
55	0.1438	0.0027
57	0.1434	0.0026
59	0.1431	0.0025
61	0.1427	0.0024
63	0.1424	0.0024
65	0.1420	0.0023
67	0.1417	0.0023
69	0.1413	0.0022
71	0.1410	0.0022
73	0.1406	0.0022
75	0.1403	0.0021
77	0.1399	0.0021

Table A-2 Density variation with temperature for octadecane

Temperature (^oC)	Density, ρ (kg/m^3)	Uncertainty (kg/m^3)
27	777.2	4.5
29	776.8	4.4
31	775.6	4.1
33	774.5	3.8
35	773.3	3.6
37	772.2	3.4
39	771.0	3.2
41	769.9	3.1
43	768.7	2.9
45	767.5	2.8
47	766.3	2.8
49	765.1	2.7
51	763.9	2.7
53	762.7	2.7
55	761.5	2.7
57	760.3	2.7
59	759.1	2.8
61	757.8	2.8
63	756.6	2.9
65	755.4	2.9

Table A-3 Constant pressure specific heat capacity variation with temperature for octadecane

Temperature (^oC)	Heat capacity, Cp (J/K/mol)	Uncertainty (J/K-mol)
27	416.3	4.2
29	418.6	4.2
31	420.9	4.2
33	423.1	4.2
35	425.4	4.3
37	427.7	4.3
39	430.0	4.3
41	432.3	4.3
43	434.6	4.3
45	436.9	4.4
47	439.2	4.4
49	441.5	4.4
51	443.8	4.4
53	446.2	4.5
55	448.5	4.5
57	450.8	4.5
59	453.1	4.5
61	455.4	4.6
63	457.7	4.6
65	460.1	4.6
67	462.4	4.6
69	464.7	4.6
71	467.0	4.7
73	469.4	4.7
75	471.7	4.7

APPENDIX 2

CALIBRATION DATA FOR THETHERMOCOUPLE WIRES

RT	Reference thermometer
TW	Thermocouple wire

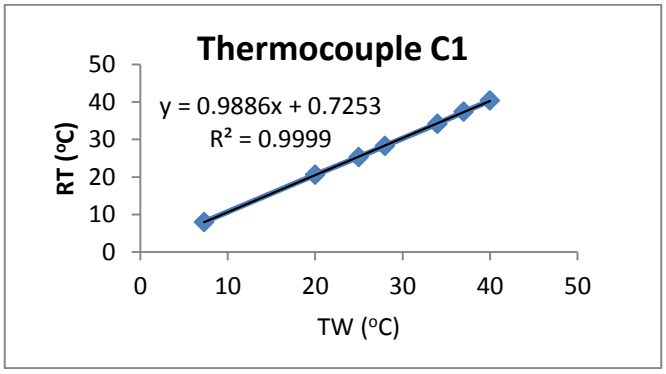

RT (^{o}C)	7.3	20.0	25.0	28.0	34.0	37.0	40.0
TW(^{o}C)	8.0	20.6	25.3	28.3	34.2	37.4	40.4

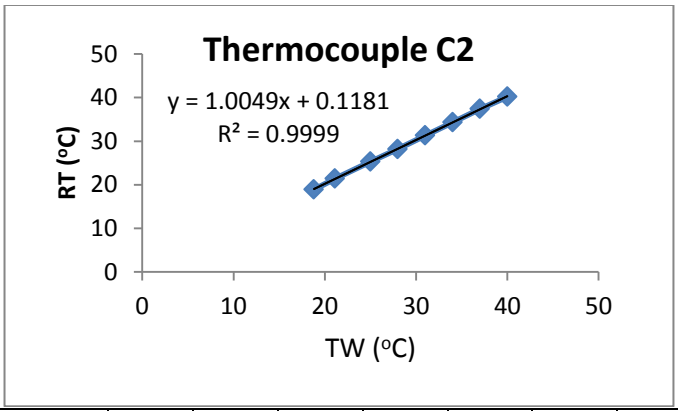

RT (^{o}C)	18.8	21.1	25.0	28.0	34.0	37.0	40.0
TW(^{o}C)	18.9	21.4	25.3	28.2	34.3	37.4	40.2

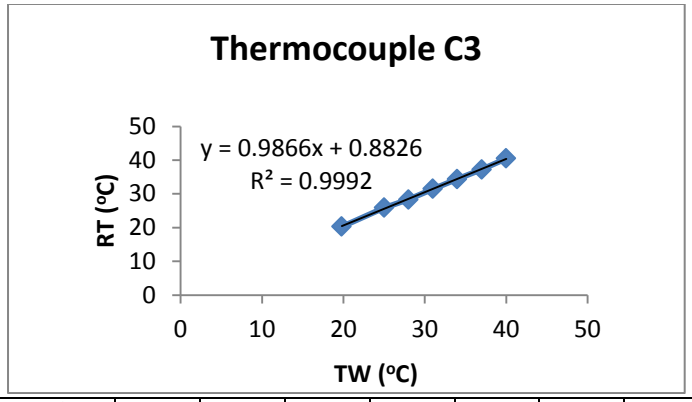

RT (^{o}C)	19.8	25.0	28.0	31.0	34.0	37.0	40.0
TW(^{o}C)	20.3	25.9	28.3	31.5	34.4	37.2	40.5

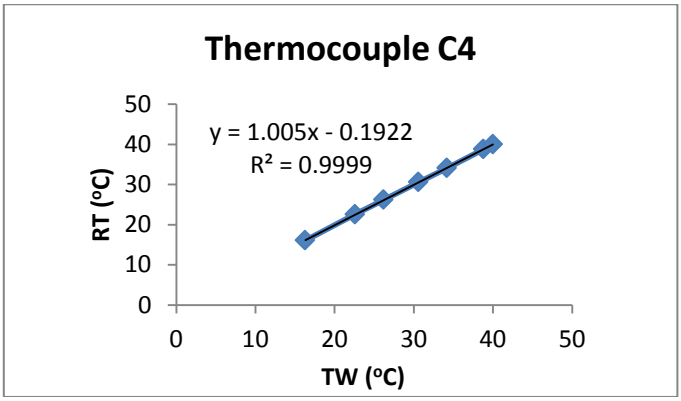

RT (^{o}C)	16.3	22.6	26.2	30.6	34.2	38.8	40.0
TW(^{o}C)	16.1	22.6	26.2	30.6	34.1	38.8	40.5

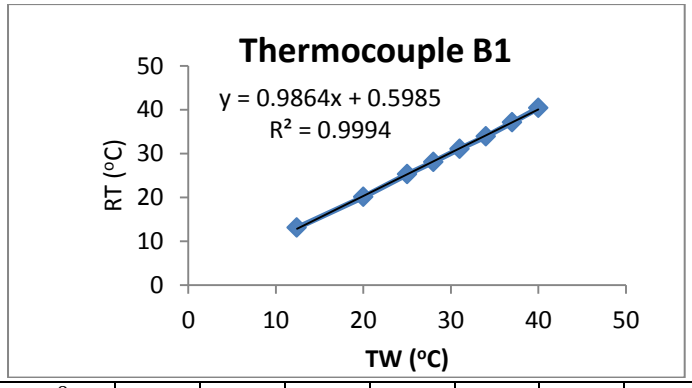

RT (^{o}C)	12.4	20.0	25.0	28.0	31.0	34.0	40.0
TW(^{o}C)	13.1	20.1	25.3	28.1	31.1	33.9	40.4

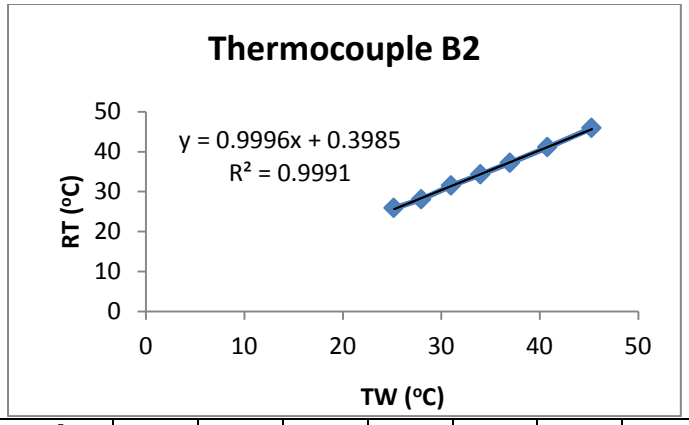

RT (^{o}C)	25.2	28.0	31.0	28.0	34.0	37.0	45.3
TW(^{o}C)	25.9	28.1	31.5	28.3	34.3	37.2	45.9

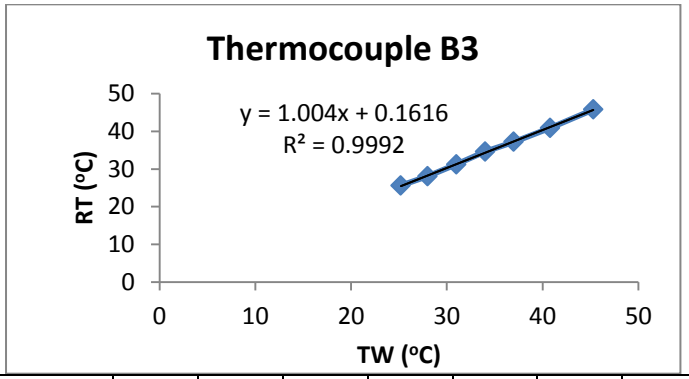

RT (^{o}C)	25.2	28.0	31.0	34.0	37.0	40.8	45.3
TW(^{o}C)	25.6	28.1	31.2	34.6	37.2	40.9	45.8

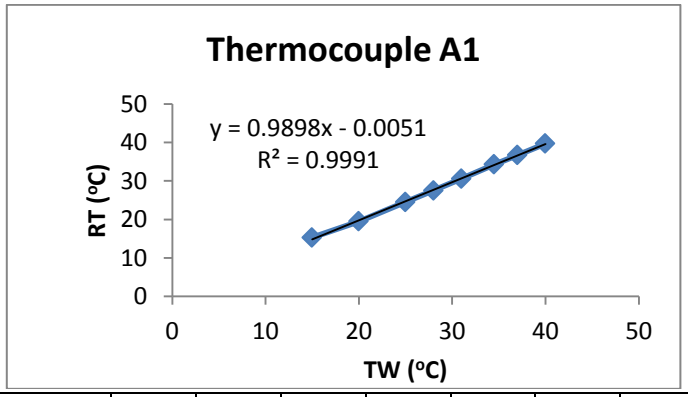

RT (^{o}C)	15.0	20.0	25.0	28.0	31.0	34.5	40.0
TW(^{o}C)	15.3	19.5	24.5	27.5	30.6	34.3	39.7

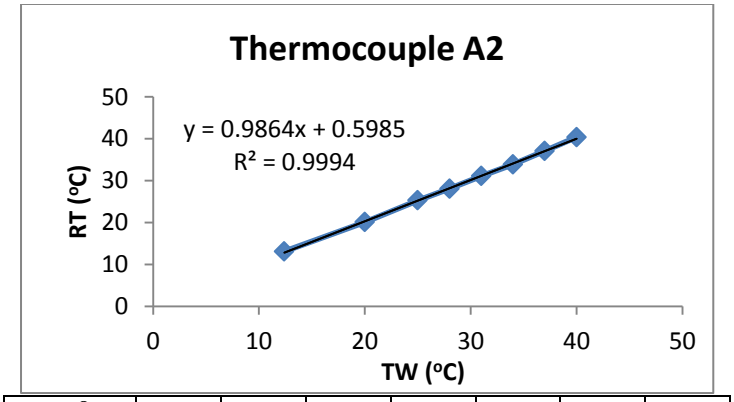

RT (^{o}C)	12.4	20.0	25.0	28.0	31.0	34.0	40.0
TW(^{o}C)	13.1	20.1	25.3	28.1	31.1	33.9	40.4

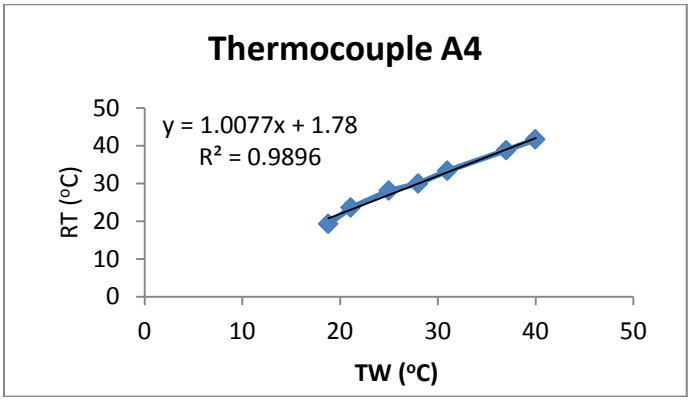

RT (^{o}C)	18.8	21.1	25.0	28.0	31.0	37.0	40.0
TW(^{o}C)	19.3	23.6	28.1	30.0	33.4	38.8	41.7

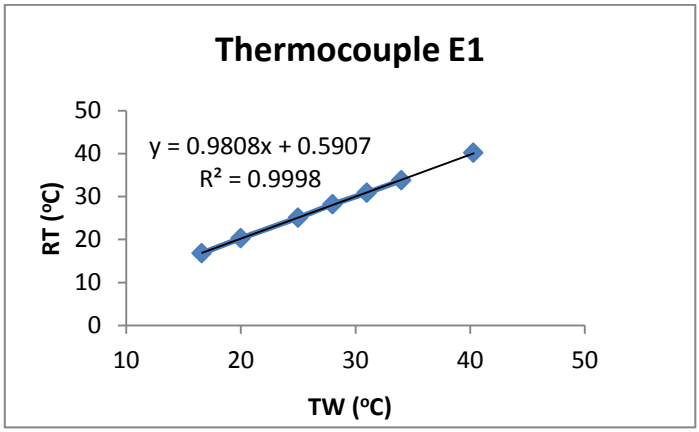

RT (^{o}C)	16.6	20.0	25.0	28.0	31.0	34.0	40.3
TW(^{o}C)	16.8	20.3	25.1	28.2	30.9	33.8	40.2

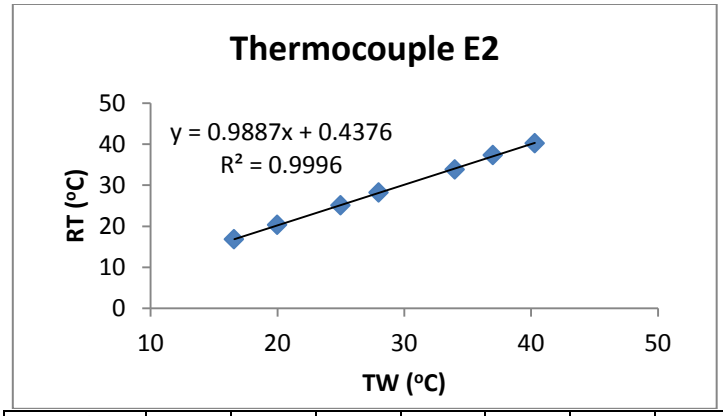

RT (^{o}C)	16.6	20.0	25.0	28.0	31.0	34.0	40.3
TW(^{o}C)	16.8	20.3	25.1	28.2	30.9	33.8	40.2

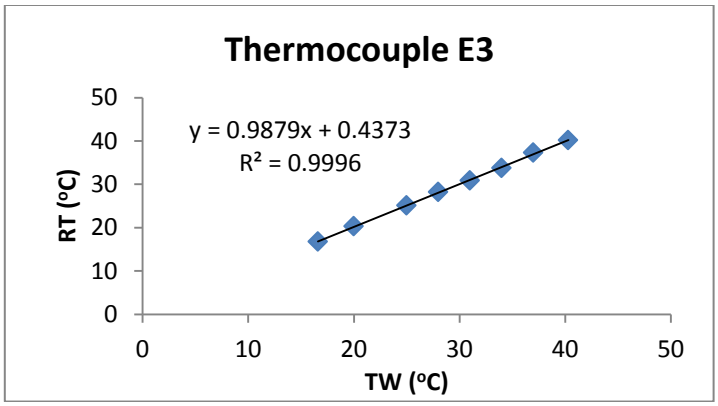

RT (^{o}C)	16.6	20.0	25.0	28.0	31.0	34.0	40.3
TW(^{o}C)	16.8	20.3	25.1	28.2	30.9	33.8	40.2

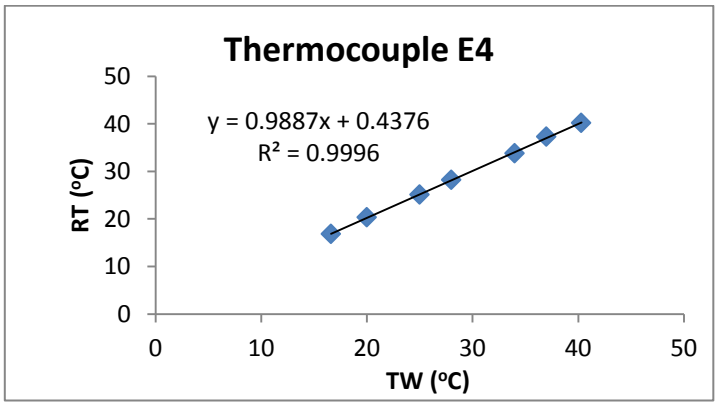

RT (^{o}C)	7.3	20.0	25.0	28.0	34.0	37.0	40.0
TW(^{o}C)	8.0	20.6	25.3	28.3	34.2	37.4	40.4

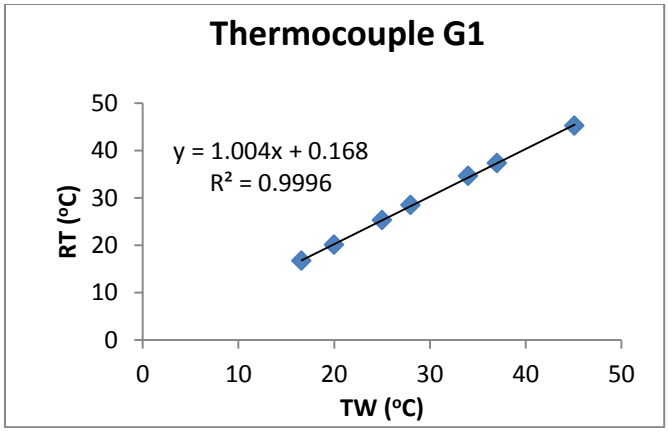

RT (^{o}C)	16.6	20.0	25.0	28.0	34.0	37.0	45.1
TW(^{o}C)	16.7	20.1	25.3	28.5	34.6	37.3	45..2

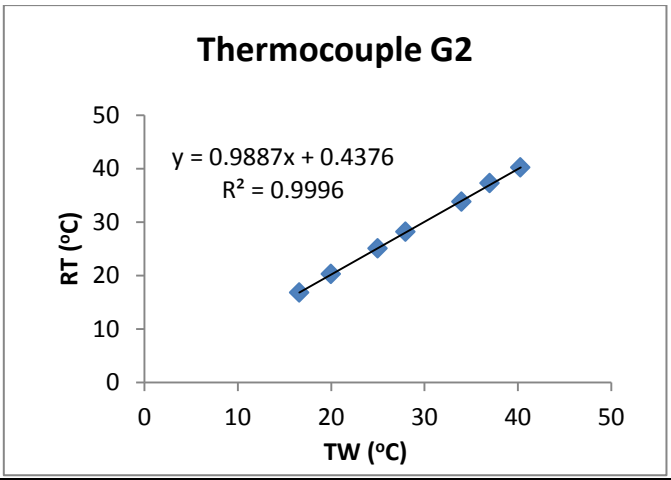

RT (^{o}C)	16.6	20.0	25.0	28.0	34.0	37.0	40.0
TW(^{o}C)	16.8	20.3	25.1	28.2	33.8	37.3	40.3

APPENDIX 3

CALIBRATION VALIDATION UNDER ISOTHERMAL CONDITIONS

Thermocouple location
Average of last 10 scans, $\overline{T_i}$
Average of last 10 scans ($\overline{T_i}$) - Grand average temperature ($\overline{\overline{T}}$)

Condition X (Grand average temperature, $\overline{\overline{T}}$ = 22.25°C)

G2	G3	E1	E2	E3	E4	C1	C2	C3	C4	B1	B2	B3	A1	A2	A4
22.22	22.24	22.28	22.28	22.26	22.28	22.38	21.90	22.01	22.31	22.15	22.20	22.35	22.41	22.39	22.39
-0.03	-0.01	0.02	0.02	0.01	0.02	0.13	-0.35	-0.24	0.05	-0.11	-0.06	0.09	0.16	0.14	0.13

Condition Y (Grand average temperature, $\overline{\overline{T}}$ = 19.89°C)

G2	G3	E1	E2	E3	E4	C1	C2	C3	C4	B1	B2	B3	A1	A2	A4
19.97	19.97	19.76	19.76	19.75	19.95	19.87	19.62	19.79	20.07	19.76	19.83	20.03	20.00	20.00	20.17
0.08	0.08	-0.13	-0.13	-0.14	0.06	-0.02	-0.27	-0.10	0.18	-0.13	-0.06	0.14	0.11	0.11	0.28

Condition Z (Grand average temperature, $\overline{\overline{T}}$ = 13.65°C)

G2	G3	E1	E2	E3	E4	C1	C2	C3	C4	B1	B2	B3	A1	A2	A4
13.45	13.44	13.55	13.58	13.63	13.71	13.76	13.36	13.71	13.86	13.59	13.61	13.82	13.77	13.82	13.89
-0.20	-0.21	-0.10	-0.07	-0.02	0.06	0.11	-0.29	0.06	0.21	-0.06	-0.04	0.17	0.12	0.17	0.24

Condition X: Just air in the TES for two days
Condition Y: 21°C water flow through TES for 10 minutes; measurement taken 2 minutes after water was drained out.
Condition Z: System filled with 11 ° C water while measurement was on-going.

APPENDIX 4

EXPERIMENTAL CONDITIONS ANALYSIS FOR COMPARISON PURPOSE

The goal of this analysis was to obtain test conditions similar to that of Agyenim et al. [54] to be applied in our TES for a valid comparison. The relationship below was assumed since the amount of heat dissipated into the PCM would depend on the amount of PCM used and the latent heat of the respective PCMs

$$\frac{\dot{Q}_{[54]}}{(m\lambda)_{[54]}} = \frac{\dot{Q}_{TES}}{(m\lambda)_{TES}} \quad (5)$$

where, the quantity $(m\lambda)$ is the amount of latent heat the PCM is capable of storing. For the multi-tube system,

$(m\lambda)_{[54]}$ = 0.057m^3 of hollow space (of multi-tube) ×1,480 kg/m^3 (density of solid Erythritol) × 80% × 339 kJ/kg (latent heat of fusion) = 22,800kJ.

80% was assumed as the fraction of the hollow space actually filled with PCM and the remaining 20% is for the free expansion of the PCM during the charging process.

$(m\lambda)_{TES}$ = 9 × 10^{-4} m^3 × 814 kg/m^3 (density of solid Octadecane) × 245kJ/kg

= 180kJ

$$\dot{Q}_{[54]} = (m\lambda)_{[54]} \times \frac{T_{melt.pt} - T_{inital}}{\Delta t} \quad (6)$$

= (0.057m^3 of hollow space (of multi-tube) × 1,480 kg/m^3 (density of solid Erythritol) × 80% × 1.38 kJ/kgK) × (118-20) ÷ 7200s = 1.3kW

The temperature gradient was taken from Fig. A-1.

Therefore using (5) above, $\dot{Q}_{TES}$ = 1.3kW × (180 ÷ 22,800) = 0.01kW

But $\dot{\dot{Q}}_{TES} = (\dot{m}c)_{TES} \times (T_{inlet} - T_{outlet})$ (7)

The only controllable parameters in the experimental setup are $\dot{m}_{TES}$ and T_{inlet}. Using energy balance, the amount of heat dissipated into the PCM from the HTF is equivalent to the sensible heat gain of the designed TES.

Therefore, $\dot{Q}_{TES} = \dot{m}_{TES} \times c_{p,w} \times (T_{inlet} - T_{outlet})$

where a ΔT of 0.8°C in (7) was assumed as the temperature drop the HTF experiences as it flows across the TES, and $c_{p,w}$= 4.12kJ/kgK,

$\dot{m}_{TES}$ = 0.0048kg/s (approximately 2 GPM)

With a slightly higher flow rate and an inlet temperature of about 31° C (30 + 0.8) for the HTF, experiment 3 was performed and the result was used to estimate ($\Delta T_{PCM}/\Delta t$) in (6).

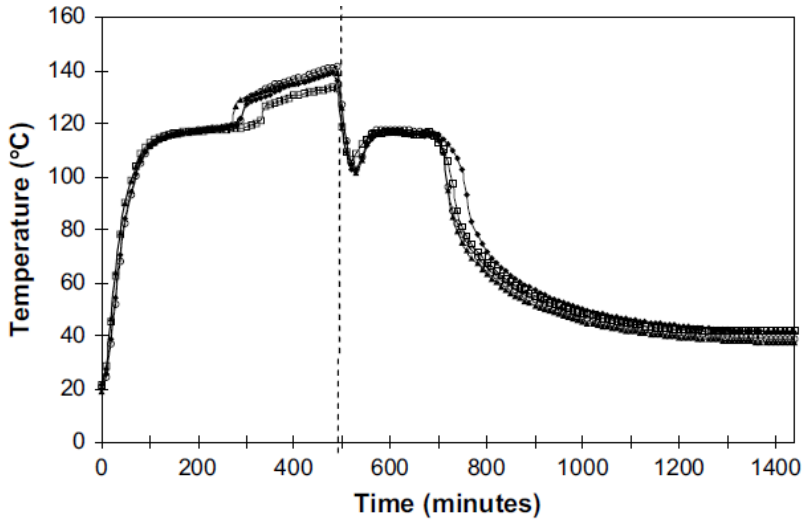

Fig. 13. The effect of mass flow rate on the average temperature in the multitube system (T_i = 140 °C).

Fig. A-1 Figure from Agyenim et al. [54]

APPENDIX 5

HYDRAULIC DIAMETER CALCULATION

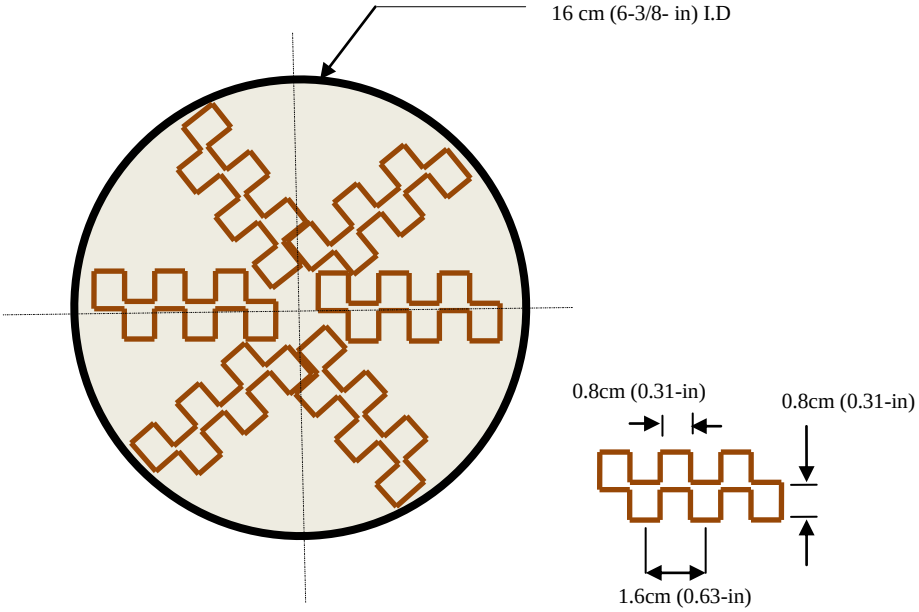

Fig. A-2 An illustration of the cross sectional view of devised TES unit

The hydraulic diameter, $D_H = \frac{4A}{P} = \frac{4\lfloor A_{shell} - A_{panels} \rfloor}{P_{shell} + P_{panels}}$

where, A is the cross sectional area and P is the wetted perimeter of the cross-section.

Total cross sectional area of all panels, A_{panels} = 6 panels × cross sectional area/panel

= 6 panels × (6 channels/panel × 0.8^2cm^2/channel)

= 23 cm^2

Cross sectional area of the TES shell, $A_{shell} = \pi$ (I.D)^2/4 = 3.14 × 16^2 cm^2/4

= 201cm^2

Wetted perimeter for TES shell, $P_{shell} = \pi$ (I.D)

= 3.14 × 16 cm = 50.2 cm

Total wetted perimeter for all panels, P_{panels} = 6 panels × (number of sides/panel × length/side)

= 6 panels × (24 sides/panel × 0.8cm/side)

= 115.2cm

Therefore, $D_H = 4 \times (201 - 23)cm^2 \div (115.2 + 50.2)cm$

= 4.3cm (1.7-in)

VITA

Name:	Clifford Okhumeode Aigbotsua
Address:	c/o Dr. Jorge Alvarado Department of Engineering Technology and Industrial Distribution Texas A&M University College Station, TX 77840-3367
Email Address:	aigbotsuaco@neo.tamu.edu
Education:	B.Sc., Mechanical Engineering, University of Lagos, Nigeria, 2006 M.S., Mechanical Engineering, Texas A&M University, USA, 2011